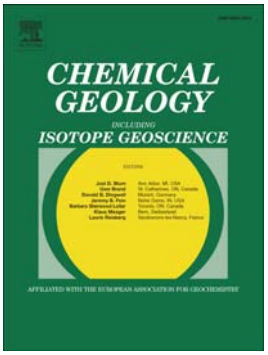

The system MgO-Al_2O_3-SiO_2 under pressure: A computational study of melting relations and phase diagrams

Donato Belmonte, Giulio Ottonello, Marino Vetuschi Zuccolini, Marco Attene

PII: S0009-2541(16)30613-1
DOI: doi: 10.1016/j.chemgeo.2016.11.011
Reference: CHEMGE 18144

To appear in: *Chemical Geology*

Received date: 26 February 2016
Revised date: 18 October 2016
Accepted date: 9 November 2016

Please cite this article as: Belmonte, Donato, Ottonello, Giulio, Zuccolini, Marino Vetuschi, Attene, Marco, The system MgO-Al_2O_3-SiO_2 under pressure: A computational study of melting relations and phase diagrams, *Chemical Geology* (2016), doi: 10.1016/j.chemgeo.2016.11.011

Published in Chemical Geology, 461 (2017) 54-64
http://dx.doi.org/10.1016/j.chemgeo.2016.11.011

The system MgO-Al_2O_3-SiO_2 under pressure: a computational study of melting relations and phase diagrams

Donato Belmonte [a,*], Giulio Ottonello [a], Marino Vetuschi Zuccolini [a], Marco Attene [b]

[a] *DISTAV, Università di Genova, Corso Europa 26, 16132 Genova, Italy*

[b] *IMATI, CNR, Via De Marini 6, 16149 Genova, Italy*

[*] Corresponding author. E-mail: donato.belmonte@unige.it

ABSTRACT

A computational scheme to predict melting phase relations in multi-component systems at high pressure and temperature is presented and applied to the MgO-Al_2O_3-SiO_2 (MAS) compositional system. A combined approach based on first principles calculations (hybrid DFT and Polarized Continuum Model), polymer chemistry (Hybrid Polymeric Approach, HPA) and equilibrium thermodynamics is developed to compute thermophysical and thermodynamic properties of the solid and liquid phases in the investigated system and infer the liquidus topology of binary and ternary phase diagrams in a broad range of P-T conditions (i.e. up to 25 GPa and 5000 K). The nature of ternary interactions in the liquid is discussed in terms of an excess Gibbs free energy contribution arising from the effect of polarization of charged species in the continuum. The computed phase diagrams show that pressure effects are able to change the nature of melting from congruent to incongruent and drastically reduce the number of solid phases with a primary phase field in the MAS system, thus leading to a remarkable simplication of melting phase relations at HP-HT. At pressures greater than 2 GPa a primary phase field of pyrope garnet opens and progressively widens from 2 to 8 GPa at the expense of those of enstatite, forsterite and spinel. Anhydrous phase B (AnhB) completely replaces forsterite on the liquidus at 9 GPa, persisting as stable liquidus phase at least up to 16-17 GPa and 2700-2750 K. At P-T conditions compatible with

the mantle transition zone, the MAS phase diagram markedly simplifies, with the three pure oxides (i.e. MgO, periclase; Al_2O_3, corundum; SiO_2, stishovite) displaying a primary phase field and majorite-pyrope garnet as the only, and most important, ternary liquidus phase in the system.

Keywords

MAS system, melting, thermodynamics, first principles, phase diagram, high pressure.

Highlights

- Melting phase relations in the MAS system are predicted through an integrated theoretical and computational approach
- Liquidus topology of binary and ternary phase diagrams is computed up to very HP-HT conditions (i.e. 25 GPa and 5000 K)
- Pressure effects produce a simplication of melting phase relations in the MAS system
- Anhydrous phase B replaces forsterite on the liquidus at P > 8 GPa
- Majorite-Pyrope garnet is the most important MAS liquidus phase at pressures between 10 and 25 GPa

1. INTRODUCTION

Understanding melting phase relations in complex geological systems is hindered by a still lacking knowledge of the thermodynamic properties of liquid and solid phases at high pressures and temperatures (HP-HT). Laboratory measurements can be applied to complex compositions and roughly constrain the onset of melting at HP-HT conditions, but they usually suffer from large uncertainties (mainly due to high thermal gradients) and rarely predict the ultimate nature of

melting. Atomistic simulations (e.g. *ab initio* or semi-empirical molecular dynamics) give useful insights on the structure-energy properties of solid and liquid phases up to very HP-HT conditions, but provide contradictory results on melting even for simple solids, like MgO (Belonoshko et al., 2010) and their application to multi-component systems is still complicated and limited by computational cost. Other empirical methods (e.g. the Lindemann criterion) can be useful to fit experimental data but, in general, are not adequate to describe the melting behaviour of minerals as they do not have a predictive power (Wolf and Jeanloz, 1984). As a matter of fact, the interpretation of melting processes at HP-HT conditions is, at present, highly speculative.

In this context, a thermodynamically-consistent computational framework is developed to predict melting phase relations in multi-component systems at high pressures and temperatures by using a combination of well-established theoretical methods (briefly described in Section 2). These methods basically provide the Gibbs free energy values of all the solid and liquid phases within a given compositional system on a grid of P-T-X conditions and allow to infer melting phase relations by minimisation algorithms. The MgO-Al_2O_3-SiO_2 (MAS) system has been chosen to test our model calculations for several reasons. First of all, this system is particularly relevant at HP-HT conditions as it accounts for ~90% of a pyrolite bulk composition (Irifune, 1987), being so a realistic proxy for a deep mantle system. Adding further chemical components to the system is expected to modify but not qualitatively change melting relations at HP-HT (Gasparik 2000, 2014). High-pressure melting relations in the MAS system provide also important clues on the generation, differentiation and crystallization behaviour of basaltic magmas and deep magma oceans in the Earth's interior (Presnall et al., 1998). Finally, MAS is a reference model system to develop high-temperature refractory ceramics and metallurgical slags (Jung et al., 2004).

High-pressure and high-temperature phase relations in MAS system have been extensively investigated at sub-solidus conditions (e.g. Schreyer and Seifert, 1969; Gasparik, 1994). There are also studies on melting relations at 1-bar pressure, based both on experimental measurements (Rankin and Merwin, 1918; Foster, 1950; Keith and Schairer, 1952; Smart and Glasser, 1976) and

thermodynamic assessments (Jung et al., 2004; Mao et al., 2005a). Nevertheless, investigations on liquidus phase relations at HP-HT conditions are limited to the relatively low-pressure range (Taylor, 1973; Milholland and Presnall, 1998; Liu and Presnall, 2000) or to sub-systems (Gasparik, 1992; Kudo and Ito, 1996). In this work we extend the thermodynamic investigation of melting relations in the MAS system to conditions relevant to a deep mantle environment (i.e. 25 GPa and 5000 K), relying on a selected dataset of computed thermodynamic and thermophysical properties of solid and liquid phases, as discussed in Section 3. The calculated phase diagrams are then used as source of information to gain new insights on the stability at liquidus of minerals up to P-T conditions compatible with the mantle transition zone (i.e. up to ~660-700 km depths).

2. THEORY AND CALCULATION METHOD

An integrated theoretical and computational approach based on first principles calculations, polymer chemistry and equilibrium thermodynamics has been developed to obtain melting phase relations in multi-component systems at HP-HT. Phase diagram topology is computed in a wide range of P-T conditions by a Gibbs free energy minimisation algorithm which employs the convex-hull method to analyze equipotential surfaces in multi-component systems. The convex-hull technique is described elsewhere (e.g. Attene and Ottonello, 2011; Natali et al., 2013; Ottonello et al., 2013), while some examples on the use of this method to calculate ternary phase diagrams can be found in the literature (e.g. Connolly and Kerrick, 1987; Voskov and Voronin, 2010; Voskov et al., 2015).

Heat capacity (C_P), standard-state entropy ($S^0_{298.15}$) and enthalpy of formation from the elements ($H^0_{f,298.15}$) of the pure liquid end-member compositions (i.e. MgO, Al_2O_3 and SiO_2) have been obtained from *ab initio* structure-energy and vibrational calculations performed with the Polarized Continuum Model (PCM) (Tomasi and Persico, 1994; Ottonello et al., 2010a; Belmonte et al., 2013; see also Supplementary Material for details). Thermophysical properties and equation-of-

state parameters of the pure liquid components have been assessed in order to be consistent with the observed melting curves at HP-HT conditions (see Section 3.1).

The Gibbs free energy of mixing (G_{mixing}) of multi-component liquids is obtained via the Hybrid Polymeric Approach (HPA; Ottonello, 2005) as a sum of discrete contributions arising from different kinds of interaction among chemical species in the structure of a polymeric substance. The different energy terms are represented by a dominant chemical interaction taking place among polymeric units (structons), a subordinated interaction taking place in the cation matrix and a strain energy contribution arising from medium-range disorder of the various structons within the anion matrix, i.e:

$$G_{mixing} = G_{chemical} + G_{cat.mix-id} + G_{cat.mix-exc} + G_{strain} \quad (1)$$

Since the liquid compositions investigated in this study have only one basic oxide in the cation matrix (i.e. MgO), the second and third terms on the right-hand side of Eq. (1) are equal to zero and can be disregarded in the following. The chemical interaction between network formers (NF) and network modifiers (NM) constitutes by far the main form of energy gained (or lost) by the liquid in the mixing process. This energy can be expressed according to the Toop-Samis model (Toop and Samis, 1962a,b) as:

$$G_{chemical} = \frac{(O^-)}{2} RT \ln K_P \quad (2)$$

where $(O^-)/2$ (i.e. half the concentration of non-bridging oxygens in the melt structure) defines the number of contacts among the functionals of the polymeric units and K_P is the polymerization constant that describes the chemical energy acquired by the melt in a single interaction among different types of oxygen, i.e.:

$$K_P = \frac{(O^{2-}) \times (O^0)}{(O^-)^2} \tag{3}$$

where O^{2-} are free oxygens, O^0 bridging oxygens and O^- non-bridging oxygens. In the HPA model the polymerization constant can be expressed as:

$$\ln K_P = A/T + B \tag{4}$$

The A and B coefficients in Eq. (4) acquire a precise thermodynamic meaning since they represent the enthalpic and entropic contributions to the chemical interaction energy between NF and NM per unit mole of contacts (see Section 3.2 for further details).

If the effects of the direct interaction between network formers in the anion matrix (weighted on their fractional amount in the system) is added to the NF-NM chemical interaction along with an excess energy term related to the electrostatic interactions of the NM sub-lattice, we have:

$$G_{chemical} = \frac{(O^-)}{2} RT \ln K_P + \left[\frac{(O^-)^*}{2} RT \ln K_{IJ} \right] \left(\frac{X_{NF}}{X_{NF} + X_{NM}} \right) + G_{excess} \tag{5}$$

where X_{NF} and X_{NM} are the molar fractions of network formers and modifiers, respectively, $(O^-)^*$ is the molar amount of non-bridging oxygen involved in NF-NF interactions and K_{IJ} is the equilibrium constant defined for the I^{th} and J^{th} network-forming oxide species (i.e. Al_2O_3 and SiO_2 in the MAS system). The last term in Eq. (5) (i.e. G_{excess}) will be defined and discussed in detail in Section 3.3 as it deserves particular attention.

The Hookean strain energy contribution to G_{mixing} (i.e. G_{strain} in Eq. 1) represents the energy spent (or gained) in conforming the relative arrangement of the various polymers in the anion sub-lattice. This term is defined by following the same combinatory rules for network formers and network modifiers (Ottonello, 2005), i.e.:

$$G_{strain} = \frac{(O^-)}{2} T\eta + \left[\frac{(O^-)^*}{2} T\eta^* \right] \left(\frac{X_{NF}}{X_{NF} + X_{NM}} \right) \tag{6}$$

$$\eta = \sum_{k=0}^{n} \eta_k \cdot (2X_{NF} - 1)^k \quad (7)$$

$$\eta_0 = \eta_{0,H} - \eta_{0,S} \times T + \eta_{0,V} \times P \quad (8)$$

The procedure to obtain the strain coefficients (η and η^* in Eqs. 6-8) can be defined as an *asymmetric* Toop deconvolution because values of K_P are constant along pseudo-binaries with fixed $SiO_2/(SiO_2+Al_2O_3)$ ratio. Moreover, the interactions within the cation and anion sub-lattices are mutually unaffected with respect to each other. Calculations for the MAS system are rather simple because mixing terms in the cation matrix are absent and the phase topology is simply dictated by the contrasting Lux-Flood behaviour (Lux, 1939; Flood and Förland, 1947) of the three oxide components (i.e. the liquidus surface at 1-bar pressure is satisfactorily conformed by nine A-B-η coefficients plus the ternary electrostatic excess polarization; see Section 3).

Thermodynamic properties of all the solid phases nucleating in the system have been calculated *ab initio* by density-functional theory (DFT) or, alternatively, taken from internally-consistent thermodynamic databases. DFT calculations have been performed with the hybrid B3LYP functional (Becke, 1993) which, along with the use of large all-electron Gaussian-type basis sets, could improve the accuracy of the calculated vibrational and thermodynamic properties of Mg-Al silicates and oxides with respect to pure LDA or GGA functionals, as shown by several computational studies (e.g. Demichelis et al., 2009; De La Pierre et al., 2011; De La Pierre and Belmonte, 2016). The *ab initio* thermodynamic and thermophysical properties obtained in our previous works for the Mg_2SiO_4 polymorphs (forsterite, wadsleyite and ringwoodite) (Ottonello et al., 2009a), stishovite (Ottonello et al., 2009b), anhydrous phase B (Ottonello et al., 2010b), sapphirine (Belmonte et al., 2014), pyrope (Erba et al., 2014; De La Pierre and Belmonte, 2016), the high-pressure polymorphs of $MgSiO_3$ (HP-clinoenstatite, akimotoite, majorite and perovskite) and periclase (Belmonte, 2013, unpublished Ph.D Thesis) have been adopted in this study (Table S1 and S2 in Supplementary Material). The other thermodynamic and thermophysical data for solid phases mostly come from the assessments of Berman and coworkers (Berman et al., 1985;

Berman, 1988) and Saxena and coworkers (Saxena et al., 1993; Fabrichnaya et al., 2004), with some modifications (Tables S1 and S2, respectively). The mixing behavior of solid phases in the MAS system has been considered as ideal or, alternatively, reproduced through Redlich-Kister model equations (Redlich and Kister, 1948) (see Supplementary Material for a detailed discussion on solid-state mixing properties).

3. RESULTS AND DISCUSSION

3.1 THERMODYNAMIC PROPERTIES OF LIQUID END-MEMBER COMPOSITIONS

3.1.1. SiO_2

A previous *ab initio* investigation of the structure-energy and vibrational properties of silica clusters in a dielectric continuum through hybrid DFT gas-phase calculations coupled with a Polarized Continuum Model approach has shown that an aggregate of D_{6h} network SiO_2 units and $[SiO_4]^{4-}$ monomers locally ordered in the short-medium range reproduces well both the experimentally observed isobaric heat capacity of silica at low T and the deviation from the Debye T^3 law (Ottonello et al., 2010a). Furthermore, the rotational and translational components generate a heat capacity gap at the melting temperature (ΔC_P) which is only partly counterbalanced by the loss of coherent motion of all the atoms in the ensemble. The thermophysical parameters of liquid silica have been optimized in order to be consistent with the observed melting curves of the different SiO_2 polymorphs in the low- to high-pressure range. The guidelines of this assessment can be found elsewhere (Ottonello et al., 2013). The melting curve of SiO_2 polymorphs have been constrained according to those observed by Jackson (1976) for cristobalite and β-quartz, Dalton and Presnall (1997) for coesite and Shen and Lazor (1995) for stishovite. The adoption of *ab initio* properties for stishovite (Ottonello et al., 2009b) leads to a further improvement of the SiO_2 melting curve at HP-HT with respect to our previous investigation

(Ottonello et al., 2013). The calculated thermodynamic and thermophysical properties of liquid SiO_2 are resumed in Tables 1 and 2.

Table 1. Thermodynamic properties of pure liquid components in the MgO-Al_2O_3-SiO_2 system as assessed in this work. $H^0_{f,298}$ = enthalpy of formation from the elements at T_r = 298.15 K, P_r = 1 bar; S^0_{298} = standard-state entropy; C_P = isobaric heat capacity ($C_p = a + bT + cT^{-2} + dT^{-1/2} + eT^{-3} + fT^2 + gT^3$).

Component	$H^0_{f,298}$ (J/mol)	S^0_{298} (J/mol×K)	a	b × 10^3	c × 10^{-5}	d	e × 10^{-8}	f × 10^6	g × 10^9
MgO	-563716.5	16.725	72.708	1.8183	-13.124	-257.27	3.0899	0.379074	-0.038084
Al_2O_3	-1640114.8	6.363	167.750	4.3878	-59.551	210.180	5.332	0.0	0.0
SiO_2	-911746.2	33.887	88.455	-3.00137	-48.527	-114.33	7.2829	0.71332	0.0059239

Table 2. Thermophysical properties of pure liquid components in the MAS system as assessed in this work. V^0_{298} = molar volume at T_r = 298.15 K and P_r = 1 bar; K_0 = bulk modulus at the athermal limit (T = 0 K); K'_0 = pressure derivative of the bulk modulus; $(dK/dT)_P$ = temperature derivative of the bulk modulus; α_V = thermal expansion coefficient ($\alpha_V = \alpha_0 T + \alpha_1 + \alpha_2 T^{-1}$).

Component	V^0_{298} (cc/mol)	K_0 (GPa)	K'_0	$(dK/dT)_P$ (bar/K)	α_0 × 10^7	α_1 × 10^7	α_2 × 10^3
MgO	11.41	35.3	4.81	0.0	-0.05514	1088	8.412
Al_2O_3	37.392	5.485	19.5	0.0	-0.02145	548.2	0.0
SiO_2	27.872	5.0	15.8	0.0	-0.3611	843.1	0.0

3.1.2 Al_2O_3

The properties of liquid alumina have been investigated from first principles by Belmonte et al. (2013) with the same procedures adopted for liquid silica. Based on the computed energies and vibrational features, a 1:3 aggregate of *D3d6* positively-charged $[Al_{12}O_{11}]^{14+}$ clusters contoured by $[AlO_4]^{5-}$ units in a dielectric continuum with dielectric constant ε=4.575 provides an isochoric heat

capacity which is roughly consistent with the estimates of Castanet (1984) at high temperature and the assessment of Stebbins et al. (1984) in the intermediate temperature range.

The *ab initio* heat capacity of α-Al_2O_3 calculated by Belmonte et al. (2013) is in excellent agreement with the calorimetric assessment of Ditmars and Douglas (1971) and has been adopted in this work (see Table 1). The melting behavior of corundum at high-pressure conditions is poorly constrained. The only experimental determination made so far (Shen and Lazor, 1995) indicates a melting temperature T_{fusion} = 3525 ± 150 K at P = 25 GPa, in agreement with the molecular dynamics simulation of Ahuja et al. (1998). The melting curve has been reproduced through an assessment of the thermophysical properties of liquid Al_2O_3 (see Table 2). The average value of the assessed thermal expansion coefficient in the T range from 2000 K to 3100K (i.e. $\alpha_V = 4.9\times10^{-5}$ K^{-1}) is slightly higher than those measured by electrostatic or aerodynamic levitation techniques, ranging from 3.4×10^{-5} K^{-1} to 4.3×10^{-5} K^{-1} according to different experimental works (Glorieux et al., 1999; Paradis et al., 2004; Langstaff et al., 2013). Nevertheless, this discrepancy seems to be reasonable if compared with α_V values measured for liquid alumina by conventional container-based techniques (e.g. Kirshenbaum and Cahill, 1960), which are overestimated by an order of magnitude due to sample contamination effects.

3.1.3 MgO

First principles molecular dynamics calculations (FPMD) have been shown as liquid MgO undergoes progressive structural changes with varying P-T conditions (Karki et al., 2006). The analysis of the radial distribution function reveals a Mg-O first neighbours coordination number around 4.5 at low P, which progressively rises to 7 with increasing pressure. The results of Karki et al. (2006) prompted us to attempt a simple B3LYP-PCM vibrational calculation assuming the liquid to be composed by $[MgO_4]^{6-}$ clusters coulombically surrounded by Mg^{2+} cations in a medium with permittivity ε=13.3 and appropriate solvation radius. We set the amount of Mg^{2+}

cations with respect to $[MgO_4]^{6-}$ units in order to maintain charge neutrality. Adopting the calculated heat capacity, entropy and enthalpy values for the liquid phase (see Table 1) and the *ab initio* thermodynamic and thermophysical properties of the solid phase as calculated by Belmonte (2013) (Tables S1 and S2), we assessed the thermophysical properties of liquid MgO to reproduce its melting curve up to HP-HT conditions. The results found in the literature are controversial, as different theoretical calculations and high-pressure experiments provide melting curves which can differ from each other up to several hundreds degrees at HP-HT conditions. A melting curve consistent with the recent experimental study of Du and Lee (2014) performed up to 40 GPa and with the FPMD computations of Belonoshko et al. (2010) and de Koker et al. (2013) at higher pressures has been obtained in this work based on the equality of chemical potentials at equilibrium and through a suitable choice of the standard state volume, equation of state and thermal expansion parameters of the liquid (Table 2).

3.2 THE THREE LIMITING BINARY SYSTEMS: $MgO\text{-}SiO_2$, $Al_2O_3\text{-}SiO_2$ AND $MgO\text{-}Al_2O_3$

Interactions in the liquid state have been resolved in terms of the Hybrid Polymeric Approach (Ottonello, 2005), whose details are given in Section 2 ("*Theory and Calculation method*"). The adopted thermodynamic and thermophysical properties of all the solid phases nucleating in the MAS system are resumed in Tables S1 and S2 of Supplementary Material. The HPA parameters for the binary liquids (i.e. $MgO\text{-}SiO_2$, $Al_2O_3\text{-}SiO_2$, $MgO\text{-}Al_2O_3$) are listed in Table 3.

Table 3. Parameters of the Hybrid Polymeric Approach for the binary liquids in the MAS system as assessed in this work (see Eqs. 4, 7 and 8).

Join	$MgO\text{-}SiO_2$	$MgO\text{-}Al_2O_3$	$Al_2O_3\text{-}SiO_2$
A	-3330	-3350	0
B	-2.5	-1.74	-1.75
$\eta_{1,S}$	3[a]	-	-

$\eta_{2,H}$	-	-12	-
$\eta_{6,S}$	-10[a]	-	13[a]
$\eta_{0,V}$	-0.32[b] / -0.23[c] / -0.27[d]	-	-
$\eta_{1,V}$	0.4[b] / 0.5[c] / 0.6[d]	-	-
$\eta_{2,V}$	-0.5[c] / -0.6[d]	-	-
$\eta_{6,V}$	-0.8[a]	-	-

(a) For $X_{SiO2} \geq 0.5$; (b) At P = 5 GPa; (c) At P = 16 GPa; (d) At P = 26 GPa.

As concerning the definition of the Gibbs free energy of mixing in the liquid aggregation state (along with its enthalpic, entropic and volumetric components) we recall that the advantage of polymeric models with respect to more agnostic procedures is that the chemical interaction assumes a precise significance in terms of energy, based on the Lux-Flood acid-base reaction formalism (Lux, 1939; Flood and Förland, 1947). The number of contacts among polymer functionals (corresponding to half the molar amount of non-bridging singly-bonded oxygens, i.e. $(O^-)/2$) depends explicitly on the contrast in the donor and acceptor properties of the basic (MgO in our case) and acidic (Al_2O_3 or SiO_2) oxides in the liquid mixture, expressed in terms of Pauling's electronegativity differences or optical basicity contrast (Ottonello, 2005; and references therein). When two oxides in a binary melt differ greatly in their acid-base properties, then the interaction is expected to be almost purely enthalpic and not significantly affected by temperature. These assessments are however qualitative at best, and indirect estimates of the enthalpy of mixing per unit mole of melt ($\overline{H}_{mixing,T_f}$) may be obtained from the experimental values of the heat of fusion (ΔH_{fusion}) of solids nucleating in the binary system of interest by applying:

$$\overline{H}_{mixing,T_f} = \frac{H_{solid,T_f} + \Delta H_{fusion} - \sum_i n_i \mu^0_{i,liquid,T_f}}{\sum_i n_i} \quad (9)$$

where μ_i and n_i are the chemical potential and the number of moles per formula unit of the i^{th} oxide in the liquid and the corresponding solid, respectively. Because the polymerization constant K_P in the HPA model is expanded as in Eq. (4), the A and B coefficients acquire a precise thermodynamic significance, related to the enthalpic and entropic contributions to the chemical interaction energy between NM and NF per unit mole of contacts, respectively. By combining Eqs. (4) and (9) with the topological features of the liquidus inferred from the T-X projection of binary phase diagrams, one acquires the decoupling between (chemical) enthalpic and entropic contributions to the Gibbs free energy of mixing.

3.2.1 MgO-SiO_2

The MgO-SiO_2 phase diagram as calculated in this work is shown in Figure 1. The topological analysis of the MgO-SiO_2 liquidus at 1-bar pressure based on the experiments of Bowen and Andersen (1914) gives the HPA parameters for the liquid (i.e. A = -3.33×10^3 K and B = -2.5; Table 3). According to the calculated phase diagram, forsterite is predicted to melt congruently at T = 2166 K; on the other hand, the incongruent melting of protoenstatite occurs at T = 1828 K and $X_{SiO2} \cong 0.52$. Bowen and Andersen (1914) found a congruent melting point of forsterite at T = 2161 K and located the protoenstatite peritectic point at T = 1830 K and X_{SiO2} = 0.51. An eutectic point between protoenstatite and β-cristobalite is predicted at T = 1798 K and $X_{SiO2} \cong 0.58$; the calculated point is only slightly displaced with respect to the experimental one, located at T = 1816 K and $X_{SiO2} \cong 0.55$ (Bowen and Andersen, 1914). The presence of a liquid-liquid miscibility gap extending from $X_{SiO2} \cong 0.59$ to nearly pure X_{SiO2} is confirmed by our calculations. The calculated consolute point at T = 2244 K and $X_{SiO2} \cong 0.84$ compares well with the experimental results of Hageman and Oonk (1986) (Figure 1).

To check the soundness of our calculated phase diagram, we use the HPA parameters derived for the MgO-SiO_2 liquid in conjunction with Eq. (9) to retrieve the enthalpy of mixing of liquids of intermediate composition along the binary join from the enthalpy of fusion of the corresponding solids. Richet et al. (1993) determined for Mg_2SiO_4 an heat of fusion of 142±14 kJ/mol at 2174 K by quantitative differential thermal analysis; the NIST-JANAF tables (Chase, 1998) assign to $MgSiO_3$ an heat of fusion of 75.3 ± 20.9 kJ/mol at 1850 K. Putting these values into Eq. (9) gives the expected enthalpy of mixing per unit mole of melt, which is -10.4 ± 10.4 kJ/mol at X_{SiO2} = 0.5 and -18.5 ± 4.7 kJ/mol at X_{SiO2} =0.333. The calculated H_{mixing} by HPA model for Mg_2SiO_4 and $MgSiO_3$ at the corresponding melting temperatures (i.e. T_f = 2174 K and T_f = 1850 K, respectively) are shown in Figure 2A. Since the number of contacts $(O^-)/2$ in the liquid is nearly equivalent within this T range, the two calculated curves at 2174 K and 1850 K are almost superimposed. The calculated values for the enthalpy of fusion of Mg_2SiO_4 and $MgSiO_3$ turn out to be 154.7 kJ/mol and 66.3 kJ/mol, respectively, which are within their quite large experimental uncertainty. Our computational method thus provides a consistent partitioning between enthalpic and entropic contributions to the chemical Gibbs free energy of mixing of the melt. This is a great advantage with respect to empirical procedures based on adjustable parameters and fitting coefficients, which usually give a correct appraisal of the Gibbs free energy of mixing but often fail to correctly split G into H and S contributions.

[FIGURE 1]

[FIGURE 2]

The liquidus topology of the MgO-SiO_2 system is sensibly affected by high-pressure effects. With the increasing pressure the liquid-liquid miscibility gap progressively shrinks up to disappear above 2 GPa, in agreeemeent with the experimental observations of Hudon et al. (2004). The consolute temperature moves to slightly higher temperatures, increasing from 2244 K at 1-bar pressure to 2259 K at 1 GPa (Figure 1). One of the most striking effect is the change of melting of

the Mg_2SiO_4 orthosilicate (forsterite) and the $MgSiO_3$ metasilicate (protoenstatite at P = 1 bar and orthoenstatite at P > 1 GPa on the liquidus) from congruent to incongruent and vice versa. Although this change is confirmed by different experimental works (Dalton and Presnall, 1997; Hudon et al., 2005), the onset pressure of incongruent / congruent melting of forsterite and enstatite is still a matter of debate (see Gasparik, 2014 for a discussion). We use the experimental evidence that orthoenstatite melts congruently at P = 5 GPa (Dalton and Presnall, 1997) to set a volume of mixing for the MgO-SiO_2 liquid mixture by a three-coefficients Redlich-Kister expansion weighted on the $(O^-)/2$ contacts (i.e. $\eta_{0,V}$ = -0.32; $\eta_{1,V}$ = 0.40; $\eta_{6,V}$ = -0.80 in Eq. 8; see Table 3). The volume of mixing of the binary MgO-SiO_2 liquid as computed in this work is roughly consistent in both sign and magnitude with the FPMD results of de Koker et al. (2013): we obtain, for instance, V_{mixing} = -1.45 cm^3/mol at 5 GPa and 3000 K for liquid composition X_{SiO2} = 0.5, as compared with $V_{mixing} \cong$ -0.7 cm^3/mol at the same P-T-X conditions according to de Koker et al. (2013). Finally, the two eutectic compositions in the binary are both shifted by pressure effects, but in a different way. The eutectic point between $MgSiO_3$ and SiO_2 is only slightly affected by pressure, while the eutectic point between Mg_2SiO_4 and $MgSiO_3$ is more markedly shifted towards Mg-rich compositions (i.e. from X_{SiO2} = 0.45 at P = 5 GPa to X_{SiO2} = 0.42 at P = 25 GPa).

3.2.2 Al_2O_3-SiO_2

Besides the limiting pure phases (i.e. Al_2O_3 corundum and SiO_2 polymorphs) and the Al_2SiO_5 polymorphs, only another crystalline phase forms at liquidus in this binary system, i.e. the "*mullite*" solid mixture. Stoichiometric mullite ($Al_6Si_2O_{13}$) has been first identified by Bowen and Greig (1924) and considered to melt incongruently. Other studies described a congruent melting behaviour (e.g. Aramaki and Roy, 1962; Staronka et al., 1968), while for some authors the melting behaviour depends in a complex manner upon the cooling rate and non-stoichiometry (e.g. Chaudhury, 1987). Adopting the heat capacity of Eriksson and Pelton (1993) and the $H^0_{f,298.15}$,

$S^0_{298.15}$ values of the NIST-JANAF tables (Chase, 1998), stoichiometric mullite melts congruently at 2141 K and forms an eutectic with alumina at 2135 K and X_{SiO2}=0.35. However, as shown by Eriksson and Pelton (1993), if mullite is assumed as non-stoichiometric (i.e. $Al_IAl_{II}[Al_{0.388}Si_{0.612}]_{III}[O_{0.961}\square_{0.039}]_{5,IV}$, where I, II, III and IV indicate four different sub-lattices in the structure) then melting turns out to be incongruent and to take place at higher T (i.e. 2163 K), in closer agreement with the results of Klug et al. (1987). More recently, Mao et al. (2005b) were able to reproduce the 1-bar subsolidus phase relations in the Al_2O_3-SiO_2 system by adopting a four sublattice solution model with a Redlich-Kister regular parameterization of interactions at subsolidus. Because in this work we are mostly interested in expanding the topological investigation of phase diagrams in the MAS system at HP conditions and we need to this purpose some hints on the volume properties of the end-member components at high pressure as well, we preferred to model the energy properties of the mullite phase as a non-ideal sub-regular mixture of the pure Al_2O_3 and SiO_2 end-members, as already proposed long ago by Howald and Eliezer (1978). Details on the mixing model adopted in this work for mullite can be found in the Supplementary Material. According to our simple model, the melting behavior of the mullite solid mixture at P = 1 bar is in good agreement with the observations of Klug et al. (1987) (Figure 3). The calculated peritectic melting of mullite occurs at T = 2175 K, as compared with T = 2163 K according to Klug et al. (1987). A deep eutectic with cristobalite at X_{SiO2} = 0.95 and T = 1929 K is also predicted, not far from that experimentally determined by Aramaki and Roy (1962) (i.e. X_{SiO2} = 0.94 and T = 1914 K). Conversely, Schairer and Bowen (1955) found a lower eutectic temperature. The strain energy contribution to the Gibbs free energy of mixing of the liquid is responsible for the marked depression of the liquidus curve near the eutectic point on the silica-rich side of the phase diagram. If solid-state mixing effects are disregarded and mullite is considered as a stoichiometric compound, the melting at P = 1 bar is congruent and takes place at 2158 K; furthermore, an eutectic with corundum comes out at T = 2153 K and X_{SiO2} = 0.34.

With increasing pressure the liquidus temperatures progressively increase and the eutectic between mullite solid mixture and SiO_2 slightly shifts towards silica-rich compositions. At P ≅ 5 GPa mullite solid mixture is no more stable on the liquidus and an eutectic between corundum and SiO_2 appears in the system. Raising the pressure from P = 5 GPa to P = 25 GPa the eutectic between corundum and coesite/stishovite sensibly moves towards Al_2O_3-rich compositions, from X_{Al2O3} = 0.37 at T = 2561 K, P = 5 GPa to X_{Al2O3} = 0.85 at T = 3453 K, P = 25 GPa. At HP conditions there are virtually no effects by solid-state mixing on the liquidus topology.

[FIGURE 3]

3.2.3 MgO-Al_2O_3

The two limiting pure phases MgO (periclase) and Al_2O_3 (corundum) do not undergo any phase transition in the investigated P-T range and the only intermediate compound stable at liquidus in this binary system is the spinel solid mixture. According to Alper et al. (1962), spinel ($MgAl_2O_4$) melts congruently at 2381 K and forms an eutectic with MgO at T = 2271 K and X_{Al2O3} = 0.325. At subsolidus conditions, however, $MgAl_2O_4$ forms a solid mixture with the Al_2O_3 component. The solubility is almost complete. According to Viechnicki et al. (1974) an Al_2O_3-rich spinel solid mixture with X_{Al2O3} = 0.85 forms an eutectic with corundum at 2248 K and X_{Al2O3} = 0.90. On the other hand, several experimental works (e.g. Roy et al., 1953; Shirasuka and Yamaguchi, 1974) point out that the solubility of alumina in the solid mixture is higher at this temperature and the existence of an eutectic point is debatable. The spinel solid mixture has been modeled by Mao et al. (2005a) in the framework of a two-sublattice compound energy formalism (CEF). A four-sublattice CEF for the same substance has been more recently proposed by Zienert and Fabrichnaya (2013). Both models are obviously quite successful in depicting the internal disorder as a function of temperature and the melting behaviour due to their marked numerical freedom. However, for the very same reasons previously outlined for the Al_2O_3-SiO_2 binary we

preferred to model the energy properties of the spinel solid mixture as a simple two-component phase with mixing occurring only on a single site (see Supplementary Material for details). According to our model, the molar fraction of Al_2O_3 in the spinel solid mixture is X_{Al2O3} = 0.545 at T = 1673 K and rises progressively to X_{Al2O3} = 0.84 at T = 2173 K. As concerning the enthalpy of fusion of stoichiometric spinel (i.e. $MgAl_2O_4$), Barin (1995) gives ΔH_{fusion} = 196.648 kJ/mol at T_{fusion}= 2408 K, which is not far from the NIST-JANAF value (i.e. ΔH_{fusion} = 194.6 ± 20.9 kJ/mol; Chase, 1998). These values return an enthalpy of mixing of -12.3 kJ/mol and -14.4 ± 9.6 kJ/mol, respectively, for the $MgAl_2O_4$ liquid composition. The enthalpy of mixing of $MgAl_2O_4$ predicted by the HPA model compares well with that estimated from the experimental values of ΔH_{fusion} taken from thermodynamic tabulations (see Figure 2B). As to the limited solubility of alumina in MgO at subsolidus temperatures, this may attain ~0.07 moles of Al_2O_3 per mole of mixture at T = 2181 K (Alper et al., 1962) as reproduced by our single-site ideal mixing model (Table S3).

Accounting for the solubility of alumina in spinel and magnesium oxide has some effect on the topology of the MgO-Al_2O_3 liquidus curve at 1-bar pressure (Figure 4). If solid-state mixing effects in solid phases are neglected, the experimental results of Roy et al. (1953) are well reproduced and an eutectic between pure spinel and corundum is observed at T = 2296 K and X_{Al2O3} = 0.83. If solid-state mixing is included in the calculation, the eutectic point disappears and liquidus temperatures are somewhat higher; however, the calculated liquidus curve is in better agreement with the experimental data of Rankin and Merwin (1916) near the eutectic between spinel and periclase (i.e. between X_{Al2O3} = 0.30 and X_{Al2O3} = 0.50). The eutectic between periclase and spinel is predicted to occur at T = 2203 K and X_{Al2O3} = 0.31 if only pure compounds are considered, while it is displaced to T = 2258 K and X_{Al2O3} = 0.325 when solubility of alumina in both magnesium oxide and spinel is taken into account. Finally, while pure $MgAl_2O_4$ turns out to melt at T = 2383 K, the spinel solid mixture shows a flat maximum at T = 2398 K between X_{Al2O3} = 0.54 and X_{Al2O3} = 0.61. The effects of solid-state mixing are not negligible also at HP conditions (Figure 4).

Increasing the pressure from 1 bar to 25 GPa leads to a sub-parallel upward shift of the liquidus curve and to a progressive shrinking of the primary phase field of spinel, which is no more present at P > 12 GPa.

[FIGURE 4]

3.3 TERNARY INTERACTIONS IN THE MAS SYSTEM

The topology of the MAS system up to P = 2.1 GPa has been already anticipated by Belmonte et al. (2014) under the simplifying assumption of negligible solid-state mixing of all the crystalline phases nucleating in the system and a different assessment of ternary interactions. Here we are more concerned with ternary interactions in the MgO-Al_2O_3-SiO_2 system, which is new with respect to what proposed for the CaO-Al_2O_3-SiO_2 system (Ottonello et al., 2013). Recent applications of the Polarized Continuum Model (PCM) to silicate melts have shown that it is possible to gain new insights on the nature of solute-solvent interactions in this class of substances from first principles (Gatti et al., 2012; Ottonello and Richet, 2014; Ottonello et al., 2015). By assigning accurate solvent parameters (dielectric constant and solvation radius) it is now possible to model silicate melts as ionic liquids and to depict through PCM calculations the magnitude of the solute-solvent electrostatic interaction and its structural effects on discrete clusters immerged in a dielectric continuum. When a molecular cluster representative of the short-range structural state of a given chemical component is embedded in the dielectric medium, it is strongly stabilized by solute-solvent electrostatic terms arising from the perturbed Hamiltonian. The additional energy terms (cavitation + dispersion + repulsion) are quite subordinate and this is the only reason why, for example, tetrahedral clusters such as $[MgO_4]^{6-}$, which are unstable at the gaseous state, become stable to all extent in a MgO liquid. The permittivity of the dielectric medium has a strong stabilizing effect also on $[SiO_4]^{4-}$ groups in SiO_2 liquid (Richet and Ottonello, 2014). Obviously, exploring the details of the structure-energy properties of a multi-component MAS liquid by means

of the *ab initio* procedure adopted for its pure liquid components is too demanding from a computational point of view. We may however approximate the effect of the dielectric medium by a simple excess polarization term. We recall that, according to Maxwell's equations, when a charge *e* (taken as origin) is placed in a dielectric medium consisting of discrete ions the polarization work is:

$$W_P = -\frac{1}{2}e\varphi = -\frac{1}{2}e\sum_i \frac{\alpha_i F_i}{r_i^2} \quad (10)$$

where φ is the potential field, α_i are ionic polarizabilities of the discrete ions, r_i are their distances from the origin and F_i is the component of the total electric field directed towards the central charge. Assuming for simplicity the ionic polarizabilities and interionic distances into Eq. (10) to vary linearly with composition, the excess polarization energy (ΔG_{excess}) may be recast in terms of the total electric field components splitted into partial charges (Δ) and a scalar term (*Q*). Since the Faraday constant (F) is related to the elementary charge *e* through the Avogadro number N_A (i.e. $e = F/N_A$), we may have:

$$\Delta = \frac{X_{SiO2}\delta_{Si} \times X_{MgO}\delta_{Mg} \times 2X_{Al2O3}\delta_{Al}}{\left(X_{SiO2}\delta_{Si} \times X_{MgO}\delta_{Mg} \times 2X_{Al2O3}\delta_{Al}\right)^3} \quad (11)$$

$$\Delta G_{excess} = \Delta W_P = \frac{1}{2}Q \times \Delta \times F \quad (12)$$

where δ are the normalized partial charges of the central cations and *Q* is the scalar term returning the correct value of the interaction when expressed in Volts (i.e. $\Delta G = -nFE$). To refine the values of the partial charges in the MAS system we adopted as reference the position of the experimental invariant points according to Rankin and Merwin (1918) (namely, 5 out of 7 of their "*quintuple points*"; see Table 4). Setting for simplicity identical charges for the network formers (i.e. $\delta_{Si} = \delta_{Al} = 0.5$), the MAS topology at P = 1 bar is nicely reproduced by adopting *Q* = – 4.871 (V/J) and assuming the partial charge of the network modifiers to be unitary whenever the amount of Al_2O_3 exceeds that of MgO [i.e. $\delta_{Mg} = 1$, for $X_{MgO}/(X_{MgO}+X_{Al2O3}) \leq 0.5$] and to be reduced progressively

toward the pure MgO composition, according to $\delta_{Mg} = 1 - 0.5 \times [X_{MgO}/(X_{MgO}+X_{Al2O3}) - 0.5]$ for $X_{MgO}/(X_{MgO}+X_{Al2O3}) > 0.5$. This has most likely to do with the fact that when Al_2O_3 exceeds MgO in the liquid composition, all Mg is exhausted in charge compensation and the central charge of Al (= 0.5 and roughly corresponding to the partial Mulliken charge of Al centers in a molten alumina medium, which is equal to 0.493 according to Belmonte et al., 2013) is replaced by Al-Mg-Al centers. For practical purposes and to extend this parametrization to multi-component systems, it seems appropriate to model the partial charges in the form of a Toop's asymmetric deconvolution (see Section 2) with SiO_2 as special component. In this case the effect of the NM is evaluated along compositional sections with constant ratio of $MgO/(MgO+Al_2O_3)$. Although the excess electrostatic work seems to affect the periodicity of the aluminosilicate chains as for the CAS system (Ottonello et al., 2013), the role of MgO on the Si-Al periodicity of polymeric chains in a MAS liquid is different (i.e. less marked and non monotonic) with respect to that of CaO in a CAS liquid (Figure 5).

[FIGURE 5]

3.4 THE MAS SYSTEM UNDER PRESSURE

The MAS liquidus surface obtained at P = 1 bar via the convex-hull algorithm by sampling the compositional space with a 250×250×250 mesh and using a temperature discretization of 1 K in the 1000 K – 3000 K range is shown in Figure 6. Both the composition and the temperature of the invariant points are reproduced with reasonable accuracy (Table 4). In particular, the overall topology of the ternary phase diagram is in good agreement with experimental results (Rankin and Merwin, 1918; Foster, 1950; Keith and Schairer, 1952; Schreyer and Schairer, 1961; Smart and Glasser, 1976; Sakai and Kawasaki, 1998) and the difference in temperature between the calculated and observed invariant points (both eutectics and peritectics) is about 20 K on average.

As to topological features, different studies pointed out as sapphirine has a primary phase field in the MAS system at ambient pressure (Foster, 1950; Keith and Schairer, 1952; Smart and Glasser, 1976). According to our calculations, this small primary phase field is limited by three peritectic points occuring at temperatures between 1723 K and 1773 K (see Figure 6 and Table 4). An ideal mixing model between the two end-members $Mg_3Al_{10}SiO_{20}$ (sapphirine-351) and $Mg_4Al_8Si_2O_{20}$ (sapphirine-442) seems to be appropriate to reproduce the primary phase field of this phase (Table S3). The *ab initio* thermodynamic properties of sapphirine end-members as calculated by Belmonte et al. (2014) have been adopted also in this work, except for slight modifications in the values of $H^0_{f,298.15}$, which have been increased by +4 kJ/mol (i.e. +0.03%) and +50 kJ/mol (i.e. +0.45%), respectively (Table S3). The refinement made on the standard-state enthalpies of formation of sapphirine end-members was necessary in order to be consistent with the new assessment of the liquid ternary interactions and to take into account the solid-state mixing effects on the liquidus topology (the latter being disregarded by Belmonte et al., 2014 for the sake of simplicity). The modified values adopted in this work (i.e. $H^0_{f,298.15}$ = -11199.294 kJ/mol for sapphirine-351 and $H^0_{f,298.15}$ = -11038.028 kJ/mol for sapphirine-442) turn out to be much closer to the experimental results measured by calorimetry (e.g. $H^0_{f,298.15}$ = -11005 ± 33.5 kJ/mol obtained for sapphirine-442 by Kiseleva, 1976).

[FIGURE 6]

Table 4: Calculated *vs* experimental invariant points (ternary eutectics and peritectics) in the MAS system at P = 1 bar. Abbreviation for minerals as in Figure 6.

Invariant point	**MgO**	**Al_2O_3**	**SiO_2**	**T (K)**	**References**
Fo-Per-Sp	0.600	0.160	0.240	1977	(1)
	0.690	0.078	0.232	1948 – 1998	(2)
Px-Trd-Crd	0.240	0.090	0.670	1614	(1)
	0.295	0.105	0.599	1613 – 1629	(3,4,5)
Fo-Px-Crd	0.355	0.105	0.540	1665	(1)
	0.360	0.119	0.521	1628 – 1638	(3,4,5)

Fo-Sp-Crd	0.370	0.125	0.505	1691	(1)
	0.371	0.130	0.499	1638 – 1653	(3,6)
Mul-Trd-Crd	0.150	0.150	0.700	1709	(1)
	0.157	0.145	0.698	1693 – 1721	(2,3,5)
Mul-Sp-Crn	0.275	0.260	0.465	1851	(1)
	0.270	0.308	0.422	1818 – 1848	(5)
Sapph-Crd-Sp	0.308	0.186	0.506	1736	(1)
	0.274	0.208	0.518	1721 – 1731	(2,5)
Sapph-Crd-Mul	0.274	0.208	0.518	1750	(1)
	0.259	0.216	0.525	1728 – 1738	(2,5)
Sapph-Mul-Sp	0.278	0.220	0.502	1773	(1)
	0.270	0.233	0.497	1740 – 1758	(2,5,7)

(1) This work (2) Keith and Schairer (1952) (3) Rankin and Merwin (1918) (4) Schreyer and Schairer (1961) (5) Smart and Glasser (1976); (6) Sakai and Kawasaki (1998); (7) Foster (1950).

Increasing the pressure from 1 bar to 1.0 GPa the primary phase field of sapphirine solid mixture widens at the expense of that of cordierite, with Al-poor and Si-rich compositions stabilized by pressure effects. The topology of the computed primary phase fields at P = 1 GPa is in good agreement with the experimental results obtained at P = 1.5 GPa by Taylor (1973) with a piston-cylinder apparatus, except for an enlarged liquidus stability of the mullite solid mixture as pointed out by our modelling (Figure 7A). Taylor (1973) found sillimanite instead of mullite on the liquidus at this pressure. However, this is not in contrast with our outcomes because, as already discussed in Section 3.2.2, we consider a non-stoichiometric mullite phase and a solution model where the Al_2SiO_5 composition is intermediate between that of the Al_2O_3 and SiO_2 end-members. A direct comparison between our calculated phase diagram at 1 GPa and the experimental results obtained by Taylor (1973) at a slightly different pressure (i.e. 1.5 GPa) is justified by the fact that the latter were obtained in a piston-cylinder without producing reversals (due to nucleation difficulties) and, most of all, without any pressure correction was made. An uncertainty of ±0.5 GPa in the results of Taylor (1973) thus seems to be likely, also in view of the fact that the

estimated error on pressure determination in melting experiments performed by multi-anvil apparati is ±1 GPa on average (e.g. Liebske and Frost, 2012).

At P > 1 GPa the primary phase field of sapphirine progressively shrinks, up to disappear just beyond 2 GPa. At this pressure a new primary phase field of pyrope garnet opens, then progressively widens from 2 to 4 GPa (Figure 7B). This finding is in agreement with the melting experiments performed by Milholland and Presnall (1998) and Liu and Presnall (2000) in the CMAS system,which show an increase in size of the primary phase volume of garnet within the same pressure range. The fact that a CMAS bulk composition was considered by those experiments confirms the evidence that the analysis of liquidus phase relations in simplified compositional systems (like the MAS or even the binary sistems) can be representative also for melting processes occurring in more complex systems, especially when HP-HT conditions are taken into account.

Raising the pressure to 7 GPa, we have a further extension of the primary phase field of pyrope at the expense of those of enstatite, forsterite and spinel, which change in size and progressively shrink. At P = 8 GPa a further complexity occurs in melting relations since forsterite starts to melt incongruently to anhydrous Phase B (AnhB) plus liquid and a new primary field for AnhB appears in the phase diagram (Figure 7C). The stability of AnhB on the liquidus is not surprising since it is commonly found among the products of multi-anvil experiments performed on different bulk-rock compositions within this HP-HT range (Herzberg and Zhang, 1996; Litasov and Ohtani, 2002; Liebske and Frost, 2012). According to our calculations, AnhB completely replaces forsterite on the liquidus at P ≅ 9 GPa, then starts to melt incongruently to periclase plus liquid up to disappear at P > 17 GPa. The liquidus stability of AnhB at HP-HT conditions is thus quite relevant for the MAS system.

[FIGURE 7]

In the pressure range exceeding 17 GPa, the MAS topology becomes much simpler (Figure 8): besides the three pure oxides (i.e. MgO, periclase; Al_2O_3, corundum; and SiO_2, stishovite),

majorite-pyrope solid mixture is the only (and most important) ternary liquidus phase in the MAS system. So high-pressure effects basically lead to a simplication of melting phase relations by drastically decreasing the number of solid phases with a primary field of crystallization. Figure 8 displays the ternary liquidus projections calculated at 23 GPa. By comparing the calculated isotherms in the T range 2973 – 3190 K with the results of high-pressure melting experiments carried out in the Enstatite ($Mg_4Si_4O_{12}$) – Pyrope ($Mg_3Al_2Si_3O_{12}$) join (Kudo and Ito, 1996; Gasparik, 1992, 2014), it turns out that the liquidus temperatures predicted by our modelling for majorite-pyrope garnet are consistent with the observed ones within ± 100 K, which is roughly the experimental uncertainty for this kind of measurements at HP-HT. An intriguing feature of the MAS liquidus surface calculated at P = 23 GPa is that it displays a local maximum within the primary phase field of majorite-pyrope garnet at temperatures around 3188 K (see Figure 8). These results confirm garnet as a predominant liquidus phase for ultrabasic bulk compositions at P-T conditions compatible with the mantle transition zone. Herzberg and Zhang (1996) and Trønnes and Frost (2002) found garnet as first liquidus phase in KLB-1 peridotite and pyrolite bulk compositions at pressures of 22-23 GPa. According to these experiments KLB-1 peridotite would have liquidus temperatures between 2563 K and 2663 K. If the experimental liquidus of a simplified MAS peridotite composition is plotted on our calculated phase diagram in Figure 8, it turns out that it is exactly crossed by the 2973 K isotherm. So the freezing point depression effect due to additional chemical components (mainly FeO) in the system is estimated to be around 300-400 K for a peridotite bulk composition at P = 23 GPa. Doing the same calculation for a chondrite bulk composition at P = 25 GPa (Andrault et al., 2011) gives again an estimated value of 300-400K for the freezing point depression effect. Melting relations predicted for the MAS system in this work are thus quite insightful to more complex (and realistic) mantle compositions as well.

[FIGURE 8]

4. CONCLUSIONS

We show that melting phase relations in multi-component systems can be predicted up to very HP-HT conditions by an integrated theoretical and computational approach based on first principles calculations, polymer chemistry and equilibrium thermodynamics. Thermodynamically-consistent energy properties of MgO-Al_2O_3-SiO_2 liquid compositions have been obtained by virtue of their polymeric structure, describing the nature of ternary interactions in terms of an excess Gibbs free energy contribution arising from the effect of asymmetric polarization of charges in the continuum. The computed phase diagrams in the MAS system show that pressure effects not only shift liquidus conditions to higher temperatures but also possibly change the nature of melting of solid phases (like forsterite and enstatite) from congruent to incongruent and vice versa. Most importantly, high pressures drastically reduce the number of solid phases with a primary phase field in the MAS system, thus leading to a simplication of melting phase relations at HP-HT. The inferred melting relations at HP-HT conditions point out also that non-olivine mineralogical phases, such as anhydrous Phase B and majorite-pyrope garnet, may become relevant liquidus phases in deep mantle environments. The former completely replaces forsterite on the liquidus at P = 9 GPa, the latter is the predominant liquidus phase in MAS at P-T conditions compatible with the mantle transition zone. Although additional chemical components (like CaO, FeO, H_2O etc.) may have important effects on melting phase relations at HP-HT, the informations provided by the analysis of phase diagrams in simplified, but representative, compositional systems like the MAS constitute a sound reference to model physico-chemical properties of liquids in deep mantle environments and to extrapolate to more complex systems the overall melting behaviour of deep mantle sources by the estimation of freezing point depression effects. The common evidence of a pressure-enhanced liquidus stability of garnet in systems with increasing degree of chemical complexity supports the role of model systems like the MAS in predicting melting relations at HP-HT conditions.

ACKNOWLEDGEMENTS

Financial support by the Institut de Physique du Globe de Paris (IPGP) to D.B. (Visiting Professor Program 2016) is warmly acknowledged. This work benefits from the constructive remarks of Pascal Richet and two other anonymous reviewers which improve the quality of the manuscript.

FIGURE CAPTIONS

Figure 1. Liquidus topology of MgO-SiO_2 phase diagram from P = 1 bar to P = 25 GPa. HPA model predictions at ambient pressure (black), 1 GPa (green), 2 GPa (brown), 5 GPa (orange), 10 GPa (red), 20 GPa (purple) and 25 GPa (blue) are compared with the experimental observations of Bowen and Andersen (1914), Hageman and Hoonk (1986) at P = 1 bar and Dalton and Presnall (1997) at P = 5 GPa.

Figure 2. Enthalpy of mixing in the NM – NF binaries. A. MgO-SiO_2 system; B. MgO-Al_2O_3 system. Estimates based on the experimental enthalpies of fusion of Mg_2SiO_4, $MgSiO_3$ and $MgAl_2O_4$ according to different authors (symbols) are compared with HPA model calculations (curves in bold).

Figure 3. Liquidus topology of Al_2O_3-SiO_2 phase diagram from P = 1 bar to P = 25 GPa. HPA model predictions (colors as in Figure 1) are compared with the experimental observations of Schairer and Bowen (1955), Aramaki and Roy (1962) and Klug et al. (1987) at P = 1 bar.

Figure 4. Liquidus topology of MgO-Al_2O_3 phase diagram from P = 1 bar to P = 25 GPa. HPA model predictions (colors as in Figure 1) are compared with the experimental observations of Rankin and Merwin (1916), Roy et al. (1953) and Alper et al. (1962) at P = 1 bar. Dotted curves refer to calculations disregarding any mixing of Al_2O_3 in solid phases.

Figure 5. Unweighted contributions of NFs to the total Gibbs free energy of mixing of MAS liquid at T = 2273 K and P = 1 bar. Solid lines refer to different molar fractions of NM (i.e. MgO) in the system. Filled circles locate the minima on the curves.

Figure 6. Liquidus surface of the MAS system at P = 1 bar as calculated in this work by the convex-hull method with a 250×250×250 mesh sampling the compositional space and a T discretisation of 1 K in the 1000 K – 3000 K range. The white zones are liquid-liquid miscibility gaps (2 liquids) or unresolved flat zones (T ~ constant). Abbreviation for minerals as follows: Crd = cordierite; Crn = corundum; Fo = forsterite; Mul = mullite; Per = periclase; Px = pyroxene; Sapph = sapphirine; Sp = spinel; Trd / Crs = tridymite / cristobalite.

Figure 7. Ternary liquidus projections of the MAS system at HP-HT conditions. Cotectic/peritectic curves are indicated by black stars, which represent computed data without any kind of smoothing. (A) MAS phase diagram at P = 1 GPa; symbols represent experimental results obtained by Taylor (1973) at P = 1.5 GPa. (B) MAS phase diagram at P = 4 GPa. (C) MAS phase diagram at P = 8 GPa. Abbreviation for minerals as in Figure 6, except for AnhB = anhydrous phase B; Coe = coesite; En = enstatite; Mul(s.m.) = mullite solid mixture; Pyp = pyrope; Qtz-β = beta-quartz.

Figure 8. MAS ternary liquidus projections at P = 23 GPa. Calculated isotherms are represented by dotted lines (for clarity reason, only the 2973 - 3173 K isotherms within the primary phase field of majorite-pyrope garnet are indicated). Symbols for cotectic/peritectic curves and mineral abbreviations as in Figure 7, except for Mj-Py(s.m.) = majorite-pyrope solid mixture and Stish = stishovite. The results of melting experiments performed on the En-Pyp join (Kudo and Ito, 1996; Gasparik, 2014) and KLB-1 peridotite bulk composition (Herzberg and Zhang, 1996; Trønnes and Frost, 2002) are shown for comparison.

REFERENCES

Ahuja, R., Belonoshko, A.B., Johansson, B., 1998. Melting and liquid structure of aluminum oxide using a molecular-dynamics simulation. Phys. Rev. E **57**, 1673-1676.

Alper, A.M., McNally, R.N., Ribbe, P.H., Doman, R.C., 1962. The system MgO-$MgAl_2O_4$. J. Am. Ceram. Soc. 45, 263-268.

Andrault, D., Bolfan-Casanova, N., Lo Nigro, G., Bouhifd, M.A., Garbarino, G., Mezouar, M., 2011. Solidus and liquidus profiles of chondritic mantle: implication for melting of the Earth across its history. Earth Planet. Sci. Lett. 304, 251-259.

Aramaki, S., Roy, R., 1962. Revised Phase Diagram for the System Al_2O_3-SiO_2. J. Am. Ceram. Soc. 5, 229-242.

Attene, M., Ottonello, G., 2011. Computational geometry meets material science. ERCIM NEWS 84, 43-44.

Barin, I., 1995. Thermochemical Data of Pure Substances. VCH, Weinheim (1885 pp.).

Becke, A.D., 1993. Density functional theochemistry. III The role of exact exchange. J. Che. Phys. 98, 5648–5652.

Belmonte, D., 2013. Ab initio Thermodynamics of Deep Mantle Minerales: The System MgO-SiO_2. Unpublished Ph.D. Thesis, University of Genova.

Belmonte, D., Ottonello, G., Vetuschi Zuccolini, M., 2013. Melting of α-Al_2O_3 and vitrification of the undercooled alumina liquid: Ab initio vibrational calculations and their thermodynamic implications. J. Chem. Phys. 138, 064507, doi: 10.1063/1.4790612.

Belmonte, D., Ottonello, G., Vetuschi Zuccolini, M., 2014. Ab initio thermodynamic and thermophysical properties of sapphirine end-members in the join $Mg_4Al_8Si_2O_{20}$-$Mg_3Al_{10}SiO_{20}$. American Mineralogist 99, 1449-1461.

Belonoshko, A.B., Arapan, S., Martonak, R., Rosengren, A., 2010. MgO phase diagram from first principles in a wide pressure-temperature range. Phys. Rev. B 81, 054110.

Berman R.G., 1988. Internally consistent thermodynamic data for minerals in the system Na_2O-K_2O-CaO-MgO-FeO-Fe_2O_3-Al_2O_3-SiO_2-TiO_2-H_2O-CO_2 . J Petrol. 29, 445-522.

Berman, R.G., Brown, T.H., Greenwood, H.J., 1985. An internally consistent thermodynamic data base for minerals in the system Na_2O-K_2O-CaO-MgO-FeO-Fe_2O_3-Al_2O_3-SiO_2-TiO_2-H_2O-CO_2. Atomic Energy Canada Ltd. Tech. Rep., 377, 62 pp.

Bowen, N.L., Andersen, O., 1914. The binary system MgO - SiO_2. Am. J. Sci. 37, 487-500.

Bowen, N.L., Greig, J.W., 1924. The system Alumina-Silica. J. Am. Ceram. Soc. 7, 238–254.

Castanet, R., 1984. Selected data on the thermodynamic properties of α-alumina. High Temperatures-High Pressures 16, 449-457.

Chase Jr., M.W., 1998. NIST-JANAF Thermochemical Tables. Journal of Physics and Chemistry Reference Data. Monograph No. 9. American Chemical Society, American Institute of Physics and National Institute of Standards and Technology (1951 pp.).

Chaudhuri, S.P., 1987. Melting/decomposition of mullite: incongruent or congruent? I. Phase equilibria of the system Al_2O_3–SiO_2. Ceram. Int. 13, 167-175.

Connolly, J.A.D., Kerrick, D.M., 1987. An algorithm and computer program for calculating composition phase diagrams. CALPHAD 11, 1-55.

Dalton, J.A., Presnall, D.C., 1997. No liquid immiscibility in the system $MgSiO_3$-SiO_2 at 5.0 GPa. Geochim. Cosmochim. Acta 61, 2367-2373.

de Koker, N., Karki, B.B., Stixrude, L., 2013. Thermodynamics of the MgO-SiO_2 liquid system in Earth's lowermost mantle from first principles. Earth Planet. Sci. Lett. 361, 58-63.

De La Pierre, M., Belmonte, D., 2016. Ab initio investigation of majorite and pyrope garnets:

lattice dynamics and vibrational spectra. American Mineralogist 101, 162-174.

De La Pierre, M., Orlando, R., Maschio, L., Doll, K., Ugliengo, P., Dovesi, R., 2011. Performance of six functionals (LDA, PBE, PBESOL, B3LYP, PBE0 and WC1LYP) in the simulation of vibrational and dielectric properties of crystalline compounds. The case of forsterite Mg_2SiO_4. J. Comp. Chem. 32, 1775–1784.

Demichelis, R., Civalleri, B., Ferrabone, M., Dovesi, R., 2009. On the performance of eleven DFT functionals in the description of the vibrational properties of aluminosilicates. Int. J. Quantum Chem. 110, 406-415.

Ditmars D.A., Douglas, T.B., 1971. Measurement of the relative enthalpy of pure a-Al2O3 (NBS heat capacity and enthalpy Standard Reference Material No. 720) from 273 to 1173 K. J. Res. Natl. Bur. Standards 75A, 401-420.

Du, Z., Lee, K.K.M., 2014. High-pressure melting of MgO from (Mg,Fe)O solid solutions. Geophys. Res. Lett. 41, 1-6, doi:10.1002/2014GL061954.

Erba, A., Mahmoud, A., Belmonte, D., Dovesi, R., 2014. High pressure elastic properties of minerals from ab initio simulations: the case of pyrope, grossular and andradite silicate garnets. J. Chem. Phys. 140, 124703, doi: 10.1063/1.4869144.

Eriksson, G., Pelton, A.D., 1993. Critical evaluation and optimization of the thermodynamic properties and phase diagrams of the CaO-Al_2O_3, Al_2O_3-SiO_2 and CaO-Al_2O_3-SiO_2 systems. Metall. Trans. 24B, 807-816.

Fabrichnaya, O.B., Saxena, S.K., Richet, P., Westrum, E.F., 2004. Thermodynamic Data, Models, and Phase Diagrams in Multicomponent Oxide Systems. Springer, Berlin-Heidelberg-New York, 198 pp.

Flood, H., Förland, T., 1947. The acidic and basic properties of oxides. Acta Chem. Scand. 1, 952-1005.

Foster, W.R., 1950. Synthetic sapphirine and its stability relations in the system MgO-Al_2O_3-SiO_2. J. Geol. 58, 135-151.

Gasparik, T., 1992. Melting experiments on the enstatite-pyrope join at 80-152 kilobar. J. Geophys. Res.-Solid Earth 97, 15181-15188.

Gasparik, T., 1994. A petrogenetic grid for the system MgO-Al_2O_3-SiO_2. J. Geol. 102, 97-109.

Gasparik, T., 2000. An internally consistent thermodynamic model for the system CaO-MgO-Al_2O_3-SiO_2 derived primarily from phase equilibrium data. J. Geol. 108, 103-119.

Gasparik, T., 2014. Phase Diagrams for Geoscientists. An Atlas of the Earth's Interior – 2nd Edition. Springer, New York-Heidelberg-Dordrecht-London (462 pp.).

Gatti, C., Ottonello, G., Richet, P., 2012. Energetics and bonding in aluminosilicate rings with alkali metal and alkaline-earth metal charge-compensating cations. J. Phys. Chem. A 116, 8584-8598.

Glorieux, B., Millot, F., Rifflet, J.-C., Coutures, J.-P., 1999. Density of superheated and undercooled liquid alumina by a contactless method. Int. J. Thermophysics 20, 1085-1094.

Hageman, V.B.M., Oonk, H.A.J., 1986. Liquid immiscibility in the SiO_2 + MgO, SiO_2 + SrO, SiO_2 + LaO_3, and SiO_2 + Y_2O_3 systems. Phys. Chem. Glasses 27, 194-198.

Herzberg, C., Zhang, J., 1996. Melting experiments on anhydrous peridotite KLB-1: compositions of magmas in the upper mantle and transition zone. J. Geophys. Res.-Solid Earth 101, 8271-8295.

Howald, R.A., Eliezer, I., 1978. Thermodynamic properties of mullite. J. Phys. Chem. 82, 2199-2204.

Hudon, P., Jung, I.-H., Baker, D.R., 2004. Effect of pressure on liquid-liquid miscibility gaps: a case study of the systems $CaO-SiO_2$, $MgO-SiO_2$, and $CaMgSi_2O_6-SiO_2$. J. Geophys. Res. 109, B03207, doi:10.1029/2003JB002659.

Hudon, P., Jung, I.-H., Baker, D.R., 2005. Experimental investigation and optimization of thermodynamic properties and phase diagrams in the systems $CaO-SiO_2$, $MgO-SiO_2$, $CaMgSi_2O_6-SiO_2$ and $CaMgSi_2O_6-Mg_2SiO_4$. J. Petrol. 46, 1859-1880.

Irifune, T., 1987. An experimental investigation of the pyroxene-garnet transformation in a pyrolite composition and its bearing on the constitution of the mantle. Phys. Earth Planet. Int. 45, 324-336.

Jackson, I., 1976. Melting of the silica isotypes SiO_2, BeF_2 and GeO_2 at elevated pressures. Phys. Earth Planet. Int. 13, 218-231.

Jung, I.-H., Decterov, S.A., Pelton, A.D., 2004. Critical thermodynamic evaluation and optimization of the $MgO-Al_2O_3$, $CaO-MgO-Al_2O_3$, and $MgO-Al_2O_3-SiO_2$ systems. JPEDAV 25, 329-345.

Karki, B.B., Bhattarai, D., Stixrude, L., 2006. First-principles calculation of the structural, dynamic, and electronic properties of liquid MgO. Phys. Rev. B 73, 174208.

Keith, M.L., Schairer, J.F., 1952. The stability field of sapphirine in the system $MgO-Al_2O_3-SiO_2$. J. Geol. 60, 181-186.

Kirshenbaum, A.D., Cahill, J.A., 1960. The density of liquid aluminium oxide. J. Inorg. Nucl. Chem. 14, 283-287.

Kiseleva, I.A., 1976. Thermodynamic parameters of the natural ordered and the synthetic disordered sapphirines. Geokhimiya 2, 189-201 (in Russian).

Klug, F.J., Prochazka, S., Doremus, R.H., 1987. Alumina-silica phase diagram in the mullite region. J. Am. Ceram. Soc. 70, 750-759.

Kudo, R., Ito, E., 1996. Melting relations in the system $Mg_4Si_4O_{12}$ (En)-$Mg_3Al_2Si_3O_{12}$ (Py) at high pressures. Phys. Earth Planet. Int. 96, 159-169.

Langstaff, D., Gunn, M., Greaves, G.N., Marsing, A., Kargl, F., 2013. Aerodynamic levitator furnace for measuring thermophysical properties of refractory liquids. Rev. Sci. Instrum. 84, 124901, doi : 10.1063/1.4832115.

Liebske, C., Frost, D.J., 2012. Mg phase relations in the MgO-$MgSiO_3$ system between 16 and 26 Gpa: implications for melting in Earth's deep interior. Earth Planet. Sci. Lett. 345-348, 159-170.

Litasov. K., Ohtani, E., 2002. Phase relations and melt compositions in CMAS–pyrolite–H_2O system up to 25 GPa. Phys. Earth Planet. Int. 134, 105-127.

Liu, T.-C., Presnall, D.C., 2000. Liquidus phase relations in the system CaO-MgO-Al_2O_3-SiO_2 at 2.0 GPa: applications to basalt fractionation, eclogites, and igneous sapphirine. J. Petrol. 41, 3-20.

Lux, H.Z. (1939). Acid and bases in fused salt bath: the determination of oxygen-ion concentration. Z. Elektrochem. 45, 303-309.

Mao, H., Fabrichnaya, O., Selleby, M., Sundman, B., 2005a. Thermodynamic assessment of MgO-Al_2O_3-SiO_2 system. J. Mater. Res. 20, 975-986.

Mao, H., Selleby, M., Sundman, B., 2005b. Phase equilibria and thermodynamics in the Al_2O_3 – SiO_2 system. Modeling of mullite and liquid. J. Am. Ceram. Soc. 88, 2544-2551.

Milholland, C.S., Presnall, D.C., 1998. Liquidus phase relations in the CaO-MgO-Al_2O_3-SiO_2 system at 3.0 GPa: the aluminous pyroxene thermal divide and high-pressure fractionation of picritic and komatiitic magmas. J. Petrol. 39, 3-27.

Natali, M., Attene, M., Ottonello, G., 2013. Steepest descent paths on simplicial meshes of arbitrary dimensions. Computers & Graphics 37, 687-696.

Ottonello, G., 2005. Chemical interactions and configurational disorder in silicate melts. Annals of Geophysics 48, 561-581.

Ottonello, G., Richet, P., 2014. The solvation radius of silicate melts based on the solubility of noble gases and scaled particle theory. J. Chem. Phys. 140, 044506, doi: 10.1063/1.4862737.

Ottonello, G., Civalleri, B., Ganguly, J., Vetuschi Zuccolini, M., Noël, Y., 2009a. Thermophysical properties of the α-β-γ polymorphs of Mg_2SiO_4: a computational study. Phys. Chem. Minerals 36, 87-106.

Ottonello, G., Vetuschi Zuccolini, M., Civalleri, B., 2009b. Thermo-chemical and thermo-physical properties of stishovite: An ab-initio all-electron investigation. CALPHAD 33, 457-468.

Ottonello, G., Vetuschi Zuccolini, M., Belmonte, D., 2010a. The vibrational behaviour of silica clusters at the glass transition: Ab initio calculations and thermodynamic implications. J. Chem. Phys. 133, 104508, doi: 10.1063/1.3483195.

Ottonello, G., Civalleri, B., Ganguly, J., Perger, W.F., Belmonte, D., Vetuschi Zuccolini, M., 2010b. Thermo-chemical and thermo-physical properties of the high-pressure phase anhydrous B ($Mg_{14}Si_5O_{24}$): An ab-initio all-electron investigation. American Mineralogist 95, 563-573.

Ottonello, G., Attene, M., Ameglio, D., Belmonte, D., Vetuschi Zuccolini, M., Natali, M., 2013. Thermodynamic investigation of the CaO-Al_2O_3-SiO_2 system at high P and T through polymer chemistry and convex-hull techniques. Chem. Geol. 346, 81-92.

Ottonello, G., Richet, P., Vetuschi Zuccolini, M., 2015. The wet solidus of silica: predictions from the scaled particle theory and polarized continuum model. J. Chem. Phys. 142, 054503, doi:http://dx.doi.org/10.1063/1.4906745.

Paradis, P.-F., Ishikawa, T., Saita, Y., Yoda, S., 2004. Non-contact thermophysical property measurements of liquid and undercooled alumina. Jpn. J. Appl. Phys. 43, 1496-1500.

Presnall, D.C., Weng, Y.-H., Milholland, C.S., Walter, M.J., 1998. Liquidus phase relations in the system MgO–$MgSiO_3$ at pressures up to 25 GPa – constraints on crystallization of a molten Hadean mantle. Phys. Earth Planet. Int. 107, 83-95.

Rankin, G.A., Merwin H.E., 1916. The ternary system CaO-Al_2O_3-MgO. J. Am. Chem. Soc., 38, 568-588.

Rankin, G.A., Merwin H.E., 1918. The ternary system MgO-Al_2O_3-SiO_2. Am. J. Sci. 45, 301-325.

Redlich, O., Kister, A.T., 1948. Thermodynamics of non-electrolyte solutions: x-y-t relations in a binary system. Ind. Eng. Chem. 40, 341-345.

Richet, P., Ottonello, G., 2014. The Earth as a multiscale quatum-mechanical system. C. R. Geoscience 346, 317-325.

Richet, P., Leclerc, F., Benoist, L., 1993. Melting of forsterite and spinel, with implications for the glass transition of Mg_2SiO_4 liquid. Geophys. Res. Lett. 20, 1675-1678.

Roy, D.M., Roy, R., Osborn, E.F., 1953. The system MgO-Al_2O_3-H_2O and influence of carbonate and nitrate ions on the phase equilibria. Amer. J. Sci. 251, 337-361.

Sakai, S., Kawasaki, T., 1998. Phase relations for $Mg_3Al_2Si_3O_{12}$ (pyrope composition) in the system MgO-Al_2O_3-SiO_2 at atmospheric pressure. Ganko 93, 18-26.

Saxena, S.K., Chatterjee, N., Fei, Y., Shen, G., 1993. Thermodynamic data on oxides and silicates. Springer-Verlag, Berlin-Heidelberg-New York (164 pp.).

Schairer, J.F., Bowen, N.L., 1955. The system K_2O-Al_2O_3-SiO_2. Am. J. Sci. 253, 681-746.

Schreyer, W.J., Schairer, J.F., 1961. Compositions and structural states of anhydrous Mg-cordierites: a re-investigation of the central part of the system MgO-Al_2O_3-SiO_2. J. Petrol. 2, 324-406.

Schreyer, W., Seifert, F., 1969. High-pressure phases in the system MgO-Al_2O_3-SiO_2-H_2O. Am. J. Sci. 267A, 407-443.

Shen, G., Lazor, P., 1995. Measurement of melting temperatures of some minerals under lower mantle pressures. J. Geophys. Res.-Solid Earth 100, 17699-17713.

Shirasuka, K., Yamaguchi, G., 1974. Precise measurement of the crystal data and the solid solution range of the defective spinel, $MgO{\cdot}nAl_2O_3$. Yogyo-Kyokai-Shi, 82, 34-37.

Smart, R.M., Glasser, F.P., 1976. Phase relations of cordierite and sapphirine in the system MgO-Al_2O_3-SiO_2. J. Mater. Sci. 11, 1459-1464.

Staronka, A., Pham, H., Rolin, M., 1968. Étude du système silice-alumine par la méthode des courbes de refroidissement. Rev. Int. Hautes Temp. Refractaires 5 (2), 111-115.

Stebbins, J.F., Carmichael, I.S.E., Moret, L.K., 1984. Heat capacities and entropies of silicate liquids and glasses. Contrib. Mineral. Petrol. 86, 131-148.

Taylor, H.C.J., 1973. Melting relations in the system MgO-Al_2O_3-SiO_2 at 15 Kb. Geol. Soc. Am. Bull. 84, 1335-1348.

Tomasi J., Persico M., 1994. Molecular interactions in solution: an overview of methods based on continuous distributions of the solvent. Chem. Rev. 94, 2027-2094.

Toop, G.W., Samis, C.S., 1962a. Some new ionic concepts of silicate slags. Canad. Metall. Quart. 1, 129-152.

Toop, G.W., Samis, C.S., 1962b. Activities of ions in silicate melts. Trans. Metall. Soc. AIME 224, 878-887.

Trønnes, R.G., Frost, D.J., 2002. Peridotite melting and mineral-melt partitioning of major and minor elements at 22–24.5 GPa. Earth Planet. Sci. Lett. 197, 117-131.

Viechnicki, D., Schmid, F., McCauley, J.W., 1974. Liquidus-solidus determinations in the system $MgAl_2O_4$-Al_2O_3. J. Amer. Ceram. Soc. 57, 47-48.

Voskov, A.L., Voronin, G.F., 2010. A universal method for calculating isobaric-isothermal sections of ternary system phase diagrams. Russian J. Phys. Chem. A 84, 525-533.

Voskov, A.L., Dzuban, A.V., Maksimov, A.I., 2015. TernAPI program for the calculation of ternary phase diagrams with isolated miscibility gaps by the convex hull method. Fluid Phase Equilib. 388, 50-58.

Wolf, G.H., Jeanloz, R., 1984. Lindemann melting law: anharmonic correction and test of its validity for minerals. J. Geophys. Res. - Solid Earth 89, 7821-7835.

Zienert, T.,bFabrichnaya, O., 2013. Thermodynamic assessment and experiments in the system MgO-Al_2O_3. CALPHAD 40, 1-9.

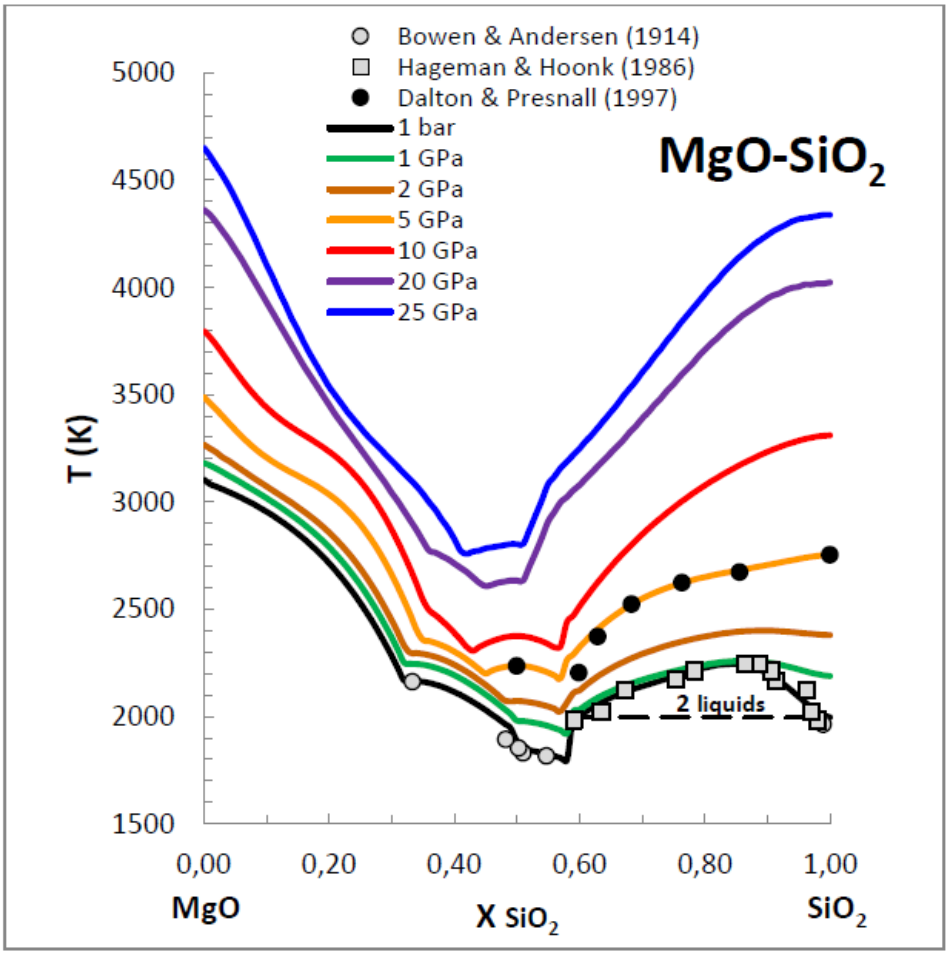

FIGURE 1

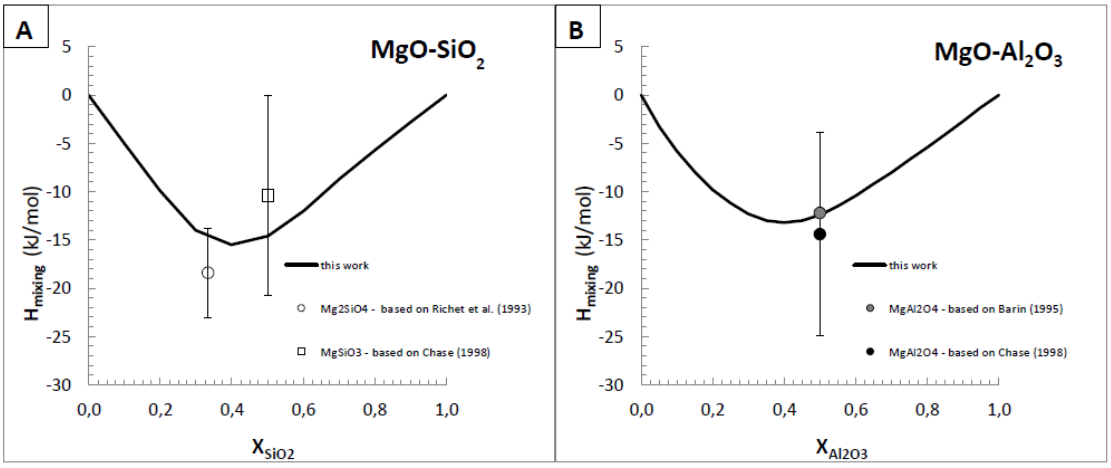

FIGURE 2

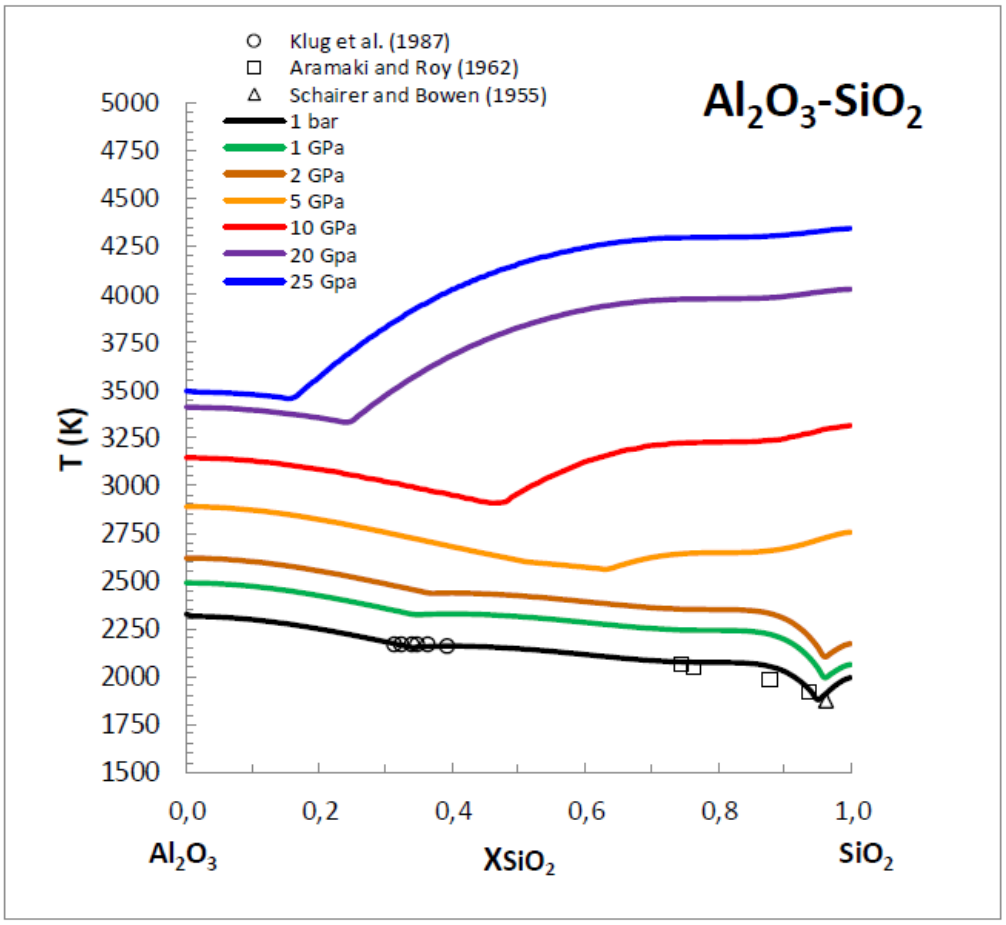

FIGURE 3

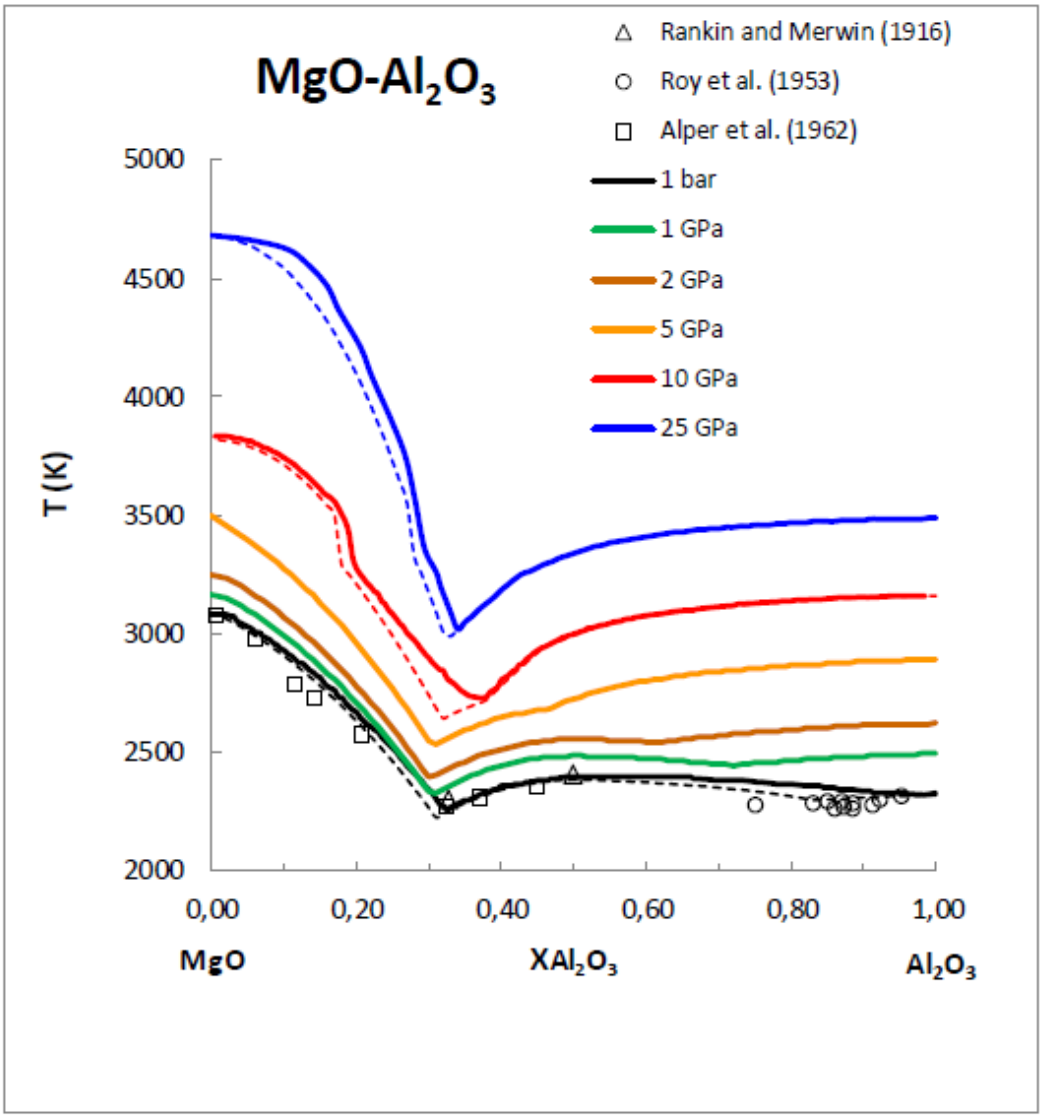

FIGURE 4

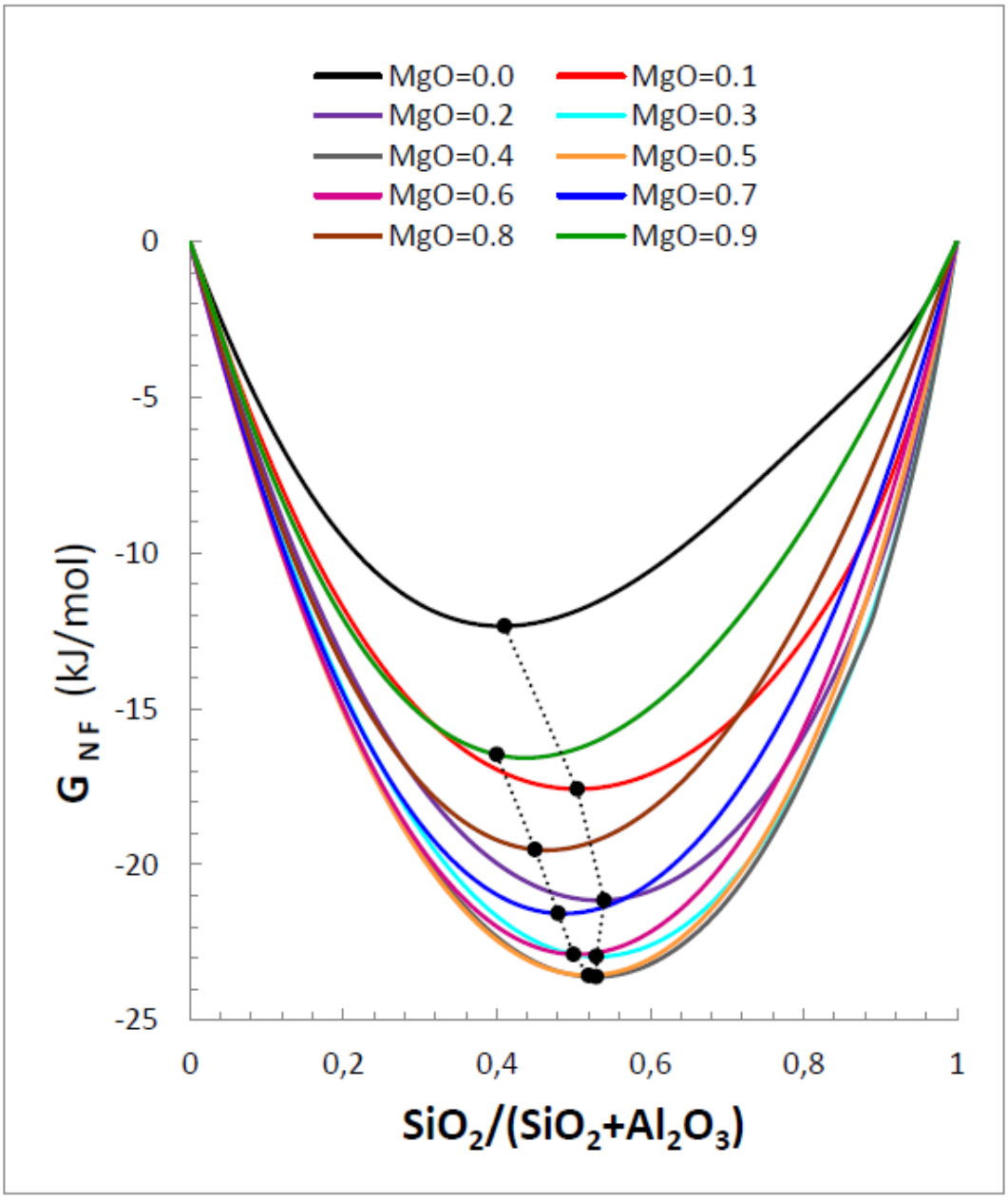

FIGURE 5

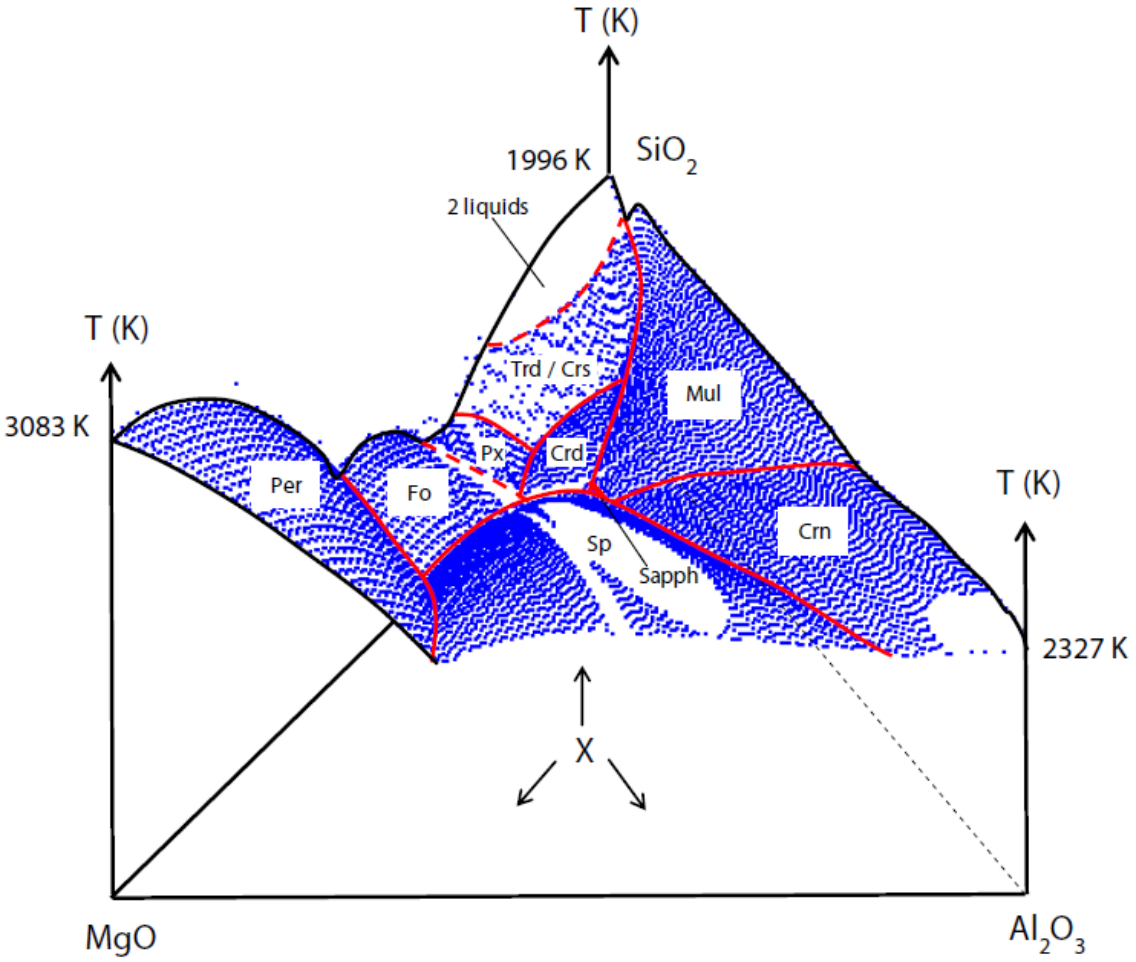

FIGURE 6

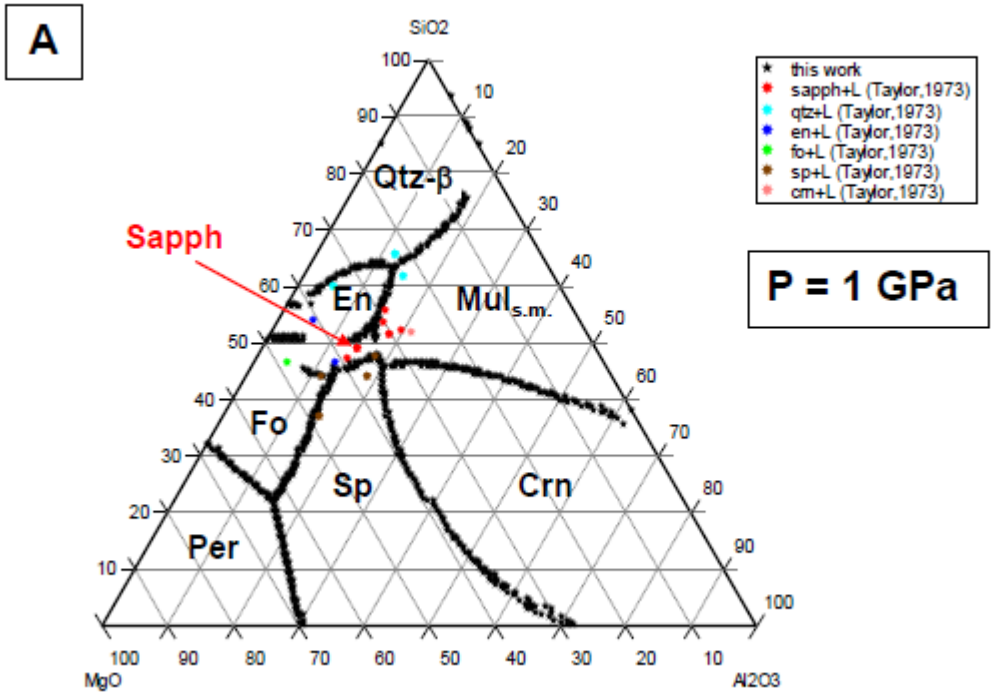

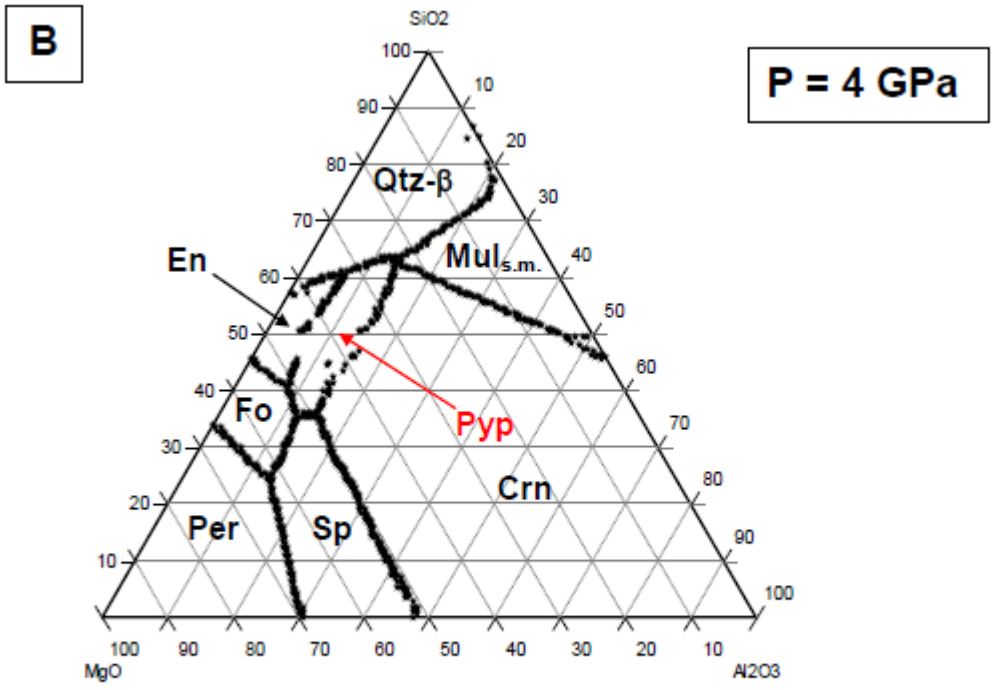

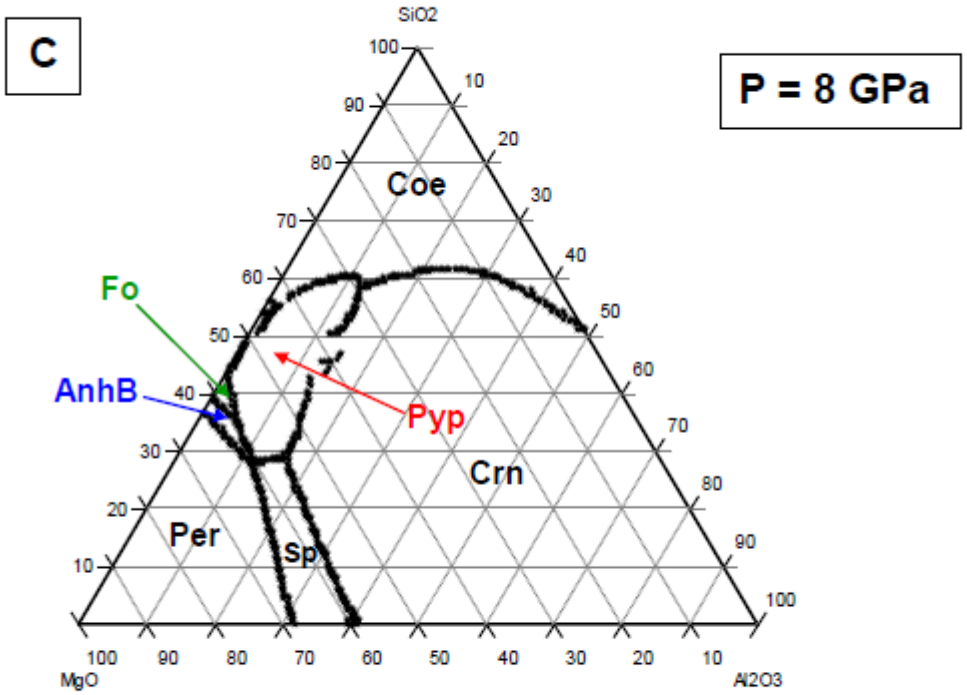

FIGURE 7

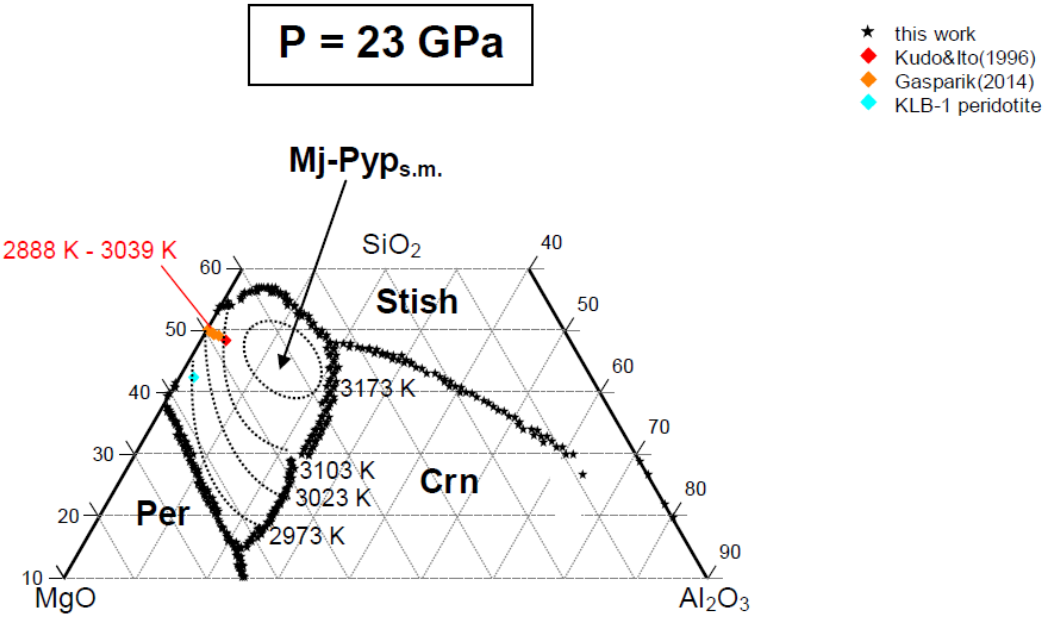

FIGURE 8